

Design of an Adaptive Controller for a Remotely Operated Air Vehicle

Luis G. Crespo*

National Institute of Aerospace, Hampton, Virginia 23666

and

Megumi Matsutani[†] and Anuradha M. Annaswamy[‡]

Massachusetts Institute of Technology, Cambridge, Massachusetts 02139

DOI: 10.2514/1.54779

This paper presents an augmented control architecture for safe flight. This architecture consists of a nominal controller that provides satisfactory performance under nominal flying conditions and a direct model reference adaptive controller that provides robustness to parametric uncertainty. The design, implementation, tuning, and robustness analysis procedures of both the nominal and augmented controllers are presented. The aim of these procedures, which encompass both theoretical and practical considerations, is to develop a controller suitable for flight. The architecture proposed is applied to the NASA generic transport model. This is a model of a transport aircraft for which both a dynamically scaled flight-test article and a high-fidelity simulation are available. A robustness analysis framework, which bounds the set of adverse flying conditions for which all closed-loop requirements are met, indicates some advantages and drawbacks of adaptation. The adverse conditions considered are grouped into four categories: aerodynamic uncertainties, structural damage, unknown time delays, and actuator failures. These failures include partial and total loss of control effectiveness, locked-in-place control surface deflections, and engine-out conditions. The requirements are fast pilot-command tracking, bounded structural loading, satisfactory transient response, bounded flight envelope, and satisfactory handling/riding qualities. A computational approach that integrates this robustness analysis framework and a design-optimization technique is proposed. This approach enables the systematic search for the controller's parameters that yield the best robustness characteristics allowed by the control structure.

I. Introduction

AN ADAPTIVE reconfigurable controller autonomously changes the controller gains to maintain satisfactory performance when unforeseen changes in the system dynamics occur. Adaptive control has the potential to improve flight safety, as it provides improved robustness and better performance to parametric uncertainty and actuator failure. Over the past three decades, adaptive control has been developed extensively and its main performance and robustness properties have been established [1–5].

In this paper we design an augmented controller for the generic transport model (GTM) developed by NASA Langley Research Center. The GTM is a model of a transport aircraft for which both a dynamically scaled flight-test article and a high-fidelity simulation are available. Figure 1 shows the flight test article and its concept of operations. References [6–8] provide details on the vehicle's configuration and characteristics, the flight experiments and the concept of operations. The aircraft is piloted from a ground station via radio frequency links by using onboard cameras and synthetic vision technology. The high-fidelity simulation uses nonlinear aerodynamic models extracted from wind-tunnel data and system identification for conditions that include high angles of attack and spins, and it considers actuator dynamics with rate and range limits,

engine dynamics, and sensor dynamics, along with analog–digital–analog latencies and quantization, sensor noise and biases, telemetry uplink and downlink time delays, turbulence, atmospheric conditions, etc. The open-loop system model has 278 state variables.

The augmented control architecture consists of a nominal controller that provides satisfactory performance under nominal flying conditions and a direct model reference adaptive controller (MRAC) that provides robustness to parametric uncertainty. The nominal controller consists of a single-point longitudinal multivariable controller having the elevator and the throttle inputs to both engines as control inputs and a single-point lateral/directional multivariable controller having the ailerons and rudders as control inputs. A fixed control allocation of this controller's outputs precludes using the engines for attitude control. On the other hand, the direct model reference adaptive controller manipulates the control surfaces and throttle inputs independently; therefore, it is solely responsible for generating thrust differentials.

Some advantages and potential drawbacks of adaptation are illustrated with point simulations. Because these simulations (as all simulations) only give a local notion of the system's robustness, the framework proposed in [9] is used to evaluate robustness from a global perspective. This framework enables sizing the set of deviations from nominal operating conditions for which the closed-loop requirements are met. This analysis is performed in a setting where most of the assumptions and simplifications supporting the control design procedure (e.g., decoupled longitudinal and lateral/directional dynamics, linear-time-invariant (LTI) plants, existence of matching conditions) do not hold. The specific adverse conditions considered can be grouped into four categories: aerodynamic uncertainties (i.e., deviations in pitch stiffness, roll, and yaw damping from nominal values), aspects of structural damage [e.g., situations where the center of gravity (c.g.) moves from its nominal location, unknown time delays, and actuator failures (e.g., situations where symmetric and asymmetric failures in control surfaces and engines occur)]. These failures include partial and total loss of control effectiveness, locked-in-place control surface deflections, and engine-out conditions. The requirements considered are fast

Presented as Paper 2010-8049 at the AIAA Guidance, Navigation, and Control Conference, Toronto, Canada; received 29 April 2011; revision received 23 August 2011; accepted for publication 3 November 2011. This material is declared a work of the U.S. Government and is not subject to copyright protection in the United States. Copies of this paper may be made for personal or internal use, on condition that the copier pay the \$10.00 per-copy fee to the Copyright Clearance Center, Inc., 222 Rosewood Drive, Danvers, MA 01923; include the code 0731-5090/12 and \$10.00 in correspondence with the CCC.

*Senior Research Scientist, 100 Exploration Way. Senior Member AIAA.

[†]Graduate Student, Aeronautics and Astronautics Department, 77 Massachusetts Avenue, Room 3-441.

[‡]Senior Research Scientist, Mechanical Engineering, 77 Massachusetts Avenue, Room 3-339A.



Fig. 1 NASA GTM test article and its concept of operations.

pilot-command tracking, bounded structural loading, bounded flight envelope (i.e., region in the state space where the aircraft dynamics are properly modeled and flying is safe), and satisfactory handling/ride qualities. Note that the controller's ability to satisfy these requirements depends on the aircraft's transient response, whose representation is mathematically intractable due to nonlinearities. Further note that these requirements define conflicting objectives. The application of this framework to a MRAC designed for the GTM illustrates some advantages and liabilities of this control architecture, as well as the risks of overturning the controller's parameters based on point simulations.

A computational approach that integrates a design-optimization technique into this robustness analysis framework is used to search for the controller's parameters that yield optimal robustness characteristics. Note that the adaptive controller's parameters, which have a significant influence on the system's response, are commonly set using ad hoc, trial and error procedures [10]. These procedures may not converge to a controller with the desired robustness characteristics. Furthermore, the determination of whether this convergence took place or not is based on computationally intensive Monte Carlo analyses. These analyses provide no guidance on how to tune the controller's parameters to achieve the desired objectives. The presence of conflicting design objectives (e.g., achieving a fast transient response and a sufficiently large time delay margin in the presence of uncertainty) further obscures the notion of causality required to deploy such methods effectively. The control tuning practice proposed herein compensates for these deficiencies by searching for controllers with improved robustness characteristics in a systematic and automated fashion.

This paper is organized as follows. Section II presents the control structure of both controllers. Section III demonstrates some advantages and potential drawbacks of adaptation via simulation. This is followed by Sec. IV where the mathematical framework supporting the robustness analysis and control tuning methods is introduced. This framework is applied to the GTM in Secs. V and VI. Finally, a few concluding remarks are given in Sec. VII.

II. Control Architecture

The system dynamics can be represented as

$$\dot{X} = F(X, \Lambda U) \quad (1)$$

where X is the state vector, U is the input vector, and $\Lambda > 0$ is the control effectiveness matrix. For control design purposes, this nonlinear plant is linearized about a trim point (X_0, U_0) satisfying $F(X_0, U_0) = 0$. Deviations from the trim values X_0 and U_0 will be written as lowercase letters hereafter: e.g., $X = X_0 + x_p$ and $U = U_0 + u$. Linearization of Eq. (1) about the trim point leads to the system

$$\dot{x}_p = A_p x_p + B_p \Lambda u + h(x_p, u) \quad (2)$$

where

$$A_p = \frac{\partial F}{\partial X} \Big|_{X_0, U_0}, \quad B_p = \frac{\partial F}{\partial U} \Big|_{X_0, U_0} \quad (3)$$

and $h(x_p, u)$ contains higher-order terms. In a sufficiently small neighborhood of the trim point the effect of the higher-order terms is negligible. The LTI representation of the plant results from dropping the higher-order terms from Eq. (2). This LTI system can be written as

$$\dot{x}_p = A_p(\hat{p})x_p + B_p \Lambda(\hat{p})(R_s(u) + d) + B_2 \hat{r} \quad (4)$$

where A_p and Λ are unknown matrices that depend on the *uncertain parameter* \hat{p} , $d(t)$ is an exogenous disturbance, \hat{r} is the reference command generated by the pilot, and $R_s(u)$ is a saturation function that enforces range saturation limits. The vector \hat{p} , which parametrizes the adverse flying conditions (i.e., aerodynamic uncertainties, damage, unknown time delays, and actuator failures), takes on the value \bar{p} when the aircraft flies under nominal operating conditions.

The state x_p consists of angle of attack α , sideslip angle β , aerodynamic speed V , roll rate p , pitch rate q , yaw rate r , longitude x , latitude y , altitude z , and the Euler angles ψ , θ , and ϕ . The control input u consists of the elevator deflection δ_e , the aileron deflection δ_a , the rudder deflection δ_r , the throttle input to the left engine δ_{thL} , and the throttle input to the right engine δ_{thR} . The reference command \hat{r} consist of angle-of-attack, sideslip, aerodynamic speed, and roll rate commands. These four commands, denoted hereafter as α_{cmd} , β_{cmd} , V_{cmd} , and p_{cmd} , are generated by the pilot to attain the desired flight maneuver. Both the nominal and adaptive controllers are based on a single trim-point design.

A. Augmented Controller

Figure 2 shows the components of the augmented control architecture. The total control input is

$$u = u_{nom} + u_{ada} \quad (5)$$

where u_{nom} is the output of the nominal controller and u_{ada} is the output of the adaptive controller. Any nominal controller, regardless of its structure and design methodology, can be augmented in the same fashion. Details of the structure of both controllers are presented next.

B. Nominal Controller

The nominal controller consists of independent controllers for the longitudinal and the lateral/directional dynamics. Both controllers assume a multivariate linear-quadratic-regulator structure with

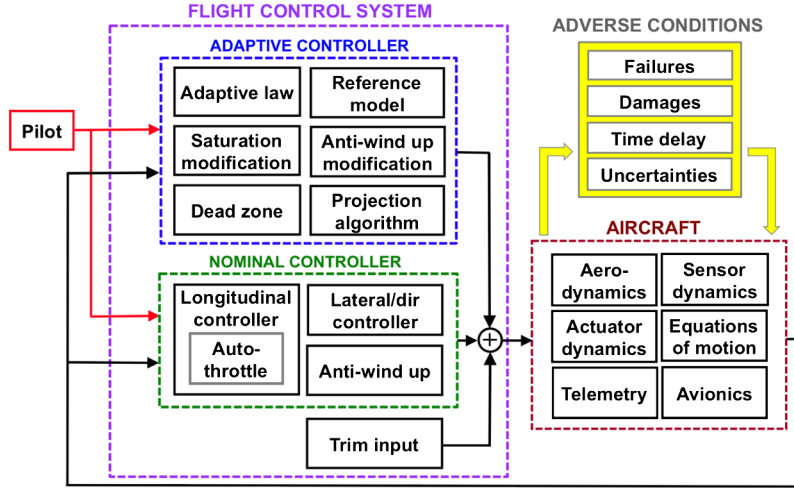


Fig. 2 Control architecture.

proportional and integral (LQR-PI) terms having integral error states for each of the components of the reference command \hat{r} . Furthermore, strategies for preventing integration windup caused by input saturation are applied. A fixed control allocation matrix that correlates inputs of the same class is used to determine the 10 main plant inputs: four elevators, two ailerons, two rudders, and two throttles. As a result, out of these 10 inputs, only four are independent.

1. Longitudinal Controller

The plant in the longitudinal axis takes the form

$$\dot{x}_{\text{lon}} = A_{\text{lon}}x_{\text{lon}} + B_{\text{lon}}u_{\text{lon}} \quad (6)$$

where $A_{\text{lon}} \in \mathbb{R}^{3 \times 3}$ is the system matrix, $B_{\text{lon}} \in \mathbb{R}^{3 \times 2}$ is the input matrix, $x_{\text{lon}} = [\alpha \ q \ V]^T$ is the state and $u_{\text{lon}} = [\delta_e \ \delta_{\text{th}}]^T$ is the input. To enable command tracking for angle of attack and airspeed, the integral error states

$$e_\alpha = \int (\alpha - \alpha_{\text{cmd}}) dt \quad (7)$$

$$e_V = \int (V - V_{\text{cmd}}) dt \quad (8)$$

are added. This leads to the augmented plant

$$\begin{bmatrix} \dot{x}_{\text{lon}} \\ \dot{e}_\alpha \\ \dot{e}_V \end{bmatrix} = \begin{bmatrix} A_{\text{lon}} & 0 \\ H_1 & 0 \end{bmatrix} \begin{bmatrix} x_{\text{lon}} \\ e_\alpha \\ e_V \end{bmatrix} + \begin{bmatrix} B_{\text{lon}} \\ 0 \end{bmatrix} \begin{bmatrix} \delta_e \\ \delta_{\text{th}} \end{bmatrix} + \begin{bmatrix} 0 \\ -I \\ 0 \end{bmatrix} \begin{bmatrix} \alpha_{\text{cmd}} \\ V_{\text{cmd}} \end{bmatrix} \quad (9)$$

where $H_1 = [[1, 0, 0]^T \ [0, 0, 0]^T \ [0, 0, 1]^T]$. A constant-gain LQR-PI controller that minimizes [ignoring the last term in Eq. (9)]

$$J = \int_0^\infty (x^T Q x + u^T R u) dt \quad (10)$$

where $Q = Q^T \geq 0$ and $R = R^T > 0$ are weighting matrices, is designed. This leads to

$$\begin{bmatrix} \delta_e \\ \delta_{\text{th}} \end{bmatrix} = [K_{\text{lon}} \ K_{e\alpha} \ K_{eV}] \begin{bmatrix} x_{\text{lon}} \\ e_\alpha \\ e_V \end{bmatrix} \quad (11)$$

This controller must attain ample stability margins so the inclusion of the low-pass- and anti-aliasing-filters from sensors and the delay caused by telemetry do not compromise stability. In particular, we use 6 dB of gain margin and 60 deg of phase margin.

The plant's input is given by

$$R_s(u) = \begin{cases} u & \text{if } u_{\min} < u < u_{\max}, \\ u_{\max} & \text{if } u \geq u_{\max}, \\ u_{\min} & \text{otherwise} \end{cases} \quad (12)$$

where u is the controller's output, and u_{\max} and u_{\min} are the saturation limits of the actuator. The control deficiency caused by this saturation function is given by

$$u_\Delta = R_s(u) - u \quad (13)$$

Details of a *resetting-based antiwindup* modification technique are presented next. The aim of antiwindup compensation is to modify the dynamics of a control loop during control saturation so that an improved transient behavior is attained after desaturation. This practice mitigates the chance of having limit cycle oscillations and successive saturation. The antiwindup technique used prevents the occurrence of excessively large controller outputs by imposing virtual saturation limits to the integral error state used for feedback. Let $\langle e, \delta \rangle$ denote a strongly coupled pair of an integral error state e and a control input δ : e.g., e_α and δ_e . The antiwindup scheme proposed is governed by the saturation function R_e defined as follows:

$$R_e(e, \delta) = \begin{cases} e & \text{if } R_2 \leq e \leq R_1, \\ R_1 & \text{if } R_1 \leq e, \\ R_2 & \text{if } e \leq R_2 \end{cases} \quad (14)$$

where the limits R_1 and R_2 are time-varying functions, assuming the smallest value of e for which the plant input is equal to any of its saturation values u_{\min} or u_{\max} . Note the similarities between Eqs. (12) and (14). The integral error state is reset to the virtual saturation limit R_1 or R_2 when $\dot{e}(t) = 0$ and either $u < u_{\min}$ or $u > u_{\max}$. Magnitude saturation limits affect the plant inputs and the antiwindup logic via Eqs. (12) and (14). Magnitude and rate saturation limits for all actuators are present in the nonlinear simulation distributed by Langley; therefore, their effects are accounted for in the robustness analysis and control tuning procedures of Sec. IV. Analogous to Eq. (13), the error deficiency caused by the antiwindup logic is

$$e_\Delta = R_e(e, \delta) - e \quad (15)$$

The saturated value of the integral error state $R_e(e)$, not the integral error state itself e , will be used for feedback. Additional details of this technique are available in [11].

In the longitudinal controller case, we apply this strategy to the $\langle e_\alpha, \delta_e \rangle$ pair. Equation (11) becomes

$$\begin{bmatrix} \delta_e \\ \delta_{\text{th}} \end{bmatrix} = [K_{\text{lon}} \quad K_{e\alpha} \quad K_{eV}] \begin{bmatrix} x_{\text{lon}} \\ R_e(e_\alpha) \\ e_V \end{bmatrix} \quad (16)$$

The effectiveness of the antiwindup scheme is a function of how well the LTI model predicts saturation and desaturation. Nonlinearities such as control surface deadband and hysteresis play a minor role in those predictions. In the case of $\langle e_V, \delta_{\text{th}} \rangle$, the highly nonlinear engine dynamics, where the thrust is a nonlinear function of the engine's rpm, make the antiwindup scheme ineffective. The determination of whether such a scheme is effective or not is based on comparing the LTI predictions with those of the coupled, fully nonlinear GTM model.

The substitutions of u with $R_s(u)$ for $u = \delta_e$ and $u = \delta_{\text{th}}$ and of e with $R_e(e, \delta)$ for $e = e_\alpha, \delta = \delta_e$ into Eq. (9) lead to

$$\begin{aligned} \begin{bmatrix} \dot{x}_{\text{lon}} \\ \dot{e}_\alpha \\ \dot{e}_V \end{bmatrix} &= \begin{bmatrix} A_{\text{lon}} + B_{\text{lon}}K_{\text{lon}} & B_{\text{lon}}K_e \\ H_1 & 0 \end{bmatrix} \begin{bmatrix} x_{\text{lon}} \\ e_\alpha \\ e_V \end{bmatrix} + \begin{bmatrix} B_{\text{lon}} \\ 0 \end{bmatrix} \begin{bmatrix} u_{\alpha,\Delta} \\ u_{V,\Delta} \end{bmatrix} \\ &+ \begin{bmatrix} B_{\text{lon}} \\ 0 \end{bmatrix} K_e \begin{bmatrix} e_{\alpha,\Delta} \\ 0 \end{bmatrix} + \begin{bmatrix} 0 \\ -I \end{bmatrix} \begin{bmatrix} \alpha_{\text{cmd}} \\ V_{\text{cmd}} \end{bmatrix} \end{aligned} \quad (17)$$

This linear time-varying system prescribes the closed-loop longitudinal dynamics with antiwindup. The boundedness of the resulting system can be established for all initial conditions inside a bounded set [12]. This bounded set extends to the entire state-space when the open-loop plant is stable and there are no unmodeled dynamics.

2. Lateral/Directional Controller

An LTI model of the corresponding plant is

$$\dot{x}_{\text{lat}} = A_{\text{lat}}x_{\text{lat}} + B_{\text{lat}}u_{\text{lat}} \quad (18)$$

where $A_{\text{lat}} \in \mathbb{R}^{3 \times 3}$ is the system matrix, $B_{\text{lat}} \in \mathbb{R}^{3 \times 2}$ is the input matrix, $x_{\text{lat}} = [\beta \quad p \quad r]^\top$ is the state, and $u_{\text{lat}} = [\delta_a \quad \delta_r]^\top$ is the input. To enable satisfactory command following, integral error states for sideslip and roll rate, given by

$$e_\beta = \int (\beta - \beta_{\text{cmd}}) dt \quad (19)$$

$$e_p = \int (p - p_{\text{cmd}}) dt \quad (20)$$

are added. The integral error in sideslip was chosen over that of the yaw rate to facilitate the generation of commands for coordinated turns with nonzero bank angles and crosswind landing. The augmented plant is given by

$$\begin{bmatrix} \dot{x}_{\text{lat}} \\ \dot{e}_\beta \\ \dot{e}_p \end{bmatrix} = \begin{bmatrix} A_{\text{lat}} & 0 \\ H_2 & 0 \end{bmatrix} \begin{bmatrix} x_{\text{lat}} \\ e_\beta \\ e_p \end{bmatrix} + \begin{bmatrix} B_{\text{lat}} \\ 0 \end{bmatrix} u_{\text{lat}} + \begin{bmatrix} 0 \\ -I \end{bmatrix} \begin{bmatrix} \beta_{\text{cmd}} \\ p_{\text{cmd}} \end{bmatrix} \quad (21)$$

where $H_2 = [[1, 0, 0]^\top \quad [0, 1, 0]^\top \quad [0, 0, 0]^\top]$. A LQR-PI control structure for the lateral controller is adopted. This leads to

$$\begin{bmatrix} \dot{\delta}_a \\ \dot{\delta}_r \end{bmatrix} = [K_{\text{lat}} \quad K_{e\beta} \quad K_{e_p}] \begin{bmatrix} x_{\text{lat}} \\ e_\beta \\ e_p \end{bmatrix} \quad (22)$$

As before, ample stability margins (e.g., 6 dB and 60 deg) should be attained to accommodate for the filters and time delays. The antiwindup technique presented earlier is applied to the $\langle e_\beta, \delta_r \rangle$ and $\langle e_p, \delta_a \rangle$ pairs. The antiwindup scheme pairs an integral error state with a control input. In its present form, this scheme requires pairing only one integral error state to a single control input. The pairs chosen exhibit the strongest dependence between the control input and the

dynamics of the integral error state; i.e., $\langle e_p, \delta_a \rangle$ is more important than $\langle e_p, \delta_r \rangle$.

3. Control Allocation

Equations (11) and (22), along with the three realizations of the antiwindup technique mentioned above, prescribe the preallocated input $u_n = [\delta_e \quad \delta_a \quad \delta_r \quad \delta_{\text{th}}]^\top$, where

$$u_n = K_n [x_{\text{lon}} \quad e_\alpha \quad e_V \quad x_{\text{lat}} \quad e_\beta \quad e_p]^\top \quad (23)$$

and $K_n \in \mathbb{R}^{4 \times 10}$ is the feedback gain. This input, along with a control allocation scheme, fully determines the 10 control inputs of the aircraft. This relationship can be written as

$$u_{\text{nom}} = G_{\text{nom}} u_n \quad (24)$$

where $G_{\text{nom}} \in \mathbb{R}^{10 \times 4}$ is the control allocation matrix. The allocation of u_n enforced by G_{nom} makes the deflection of the four elevators equal, the thrust of both engines equal, the deflection of both rudders equal, and the deflection of both ailerons equal in magnitude, having opposite directions.

C. Adaptive Controller

The second component of the architecture is an adaptive controller. The adaptive controller generates independent signals for the three main control surfaces, as well as for each throttle input. This enables using the engines for attitude control. Because of the placement of the engines and the orientation of the thrust vector relative to the c.g., changes in thrust create a pitching moment disturbance that must be cancelled by the elevators. Autothrottle designs that only depend on the aircraft velocity rely on the pilot's ability to generate a suitable set of pitch commands to attain the desired cancellation. The controller proposed pursues this cancellation automatically, thereby considerably reducing the pilot's workload. An immediate consequence of integrating the engines into the flight control system is the enlargement of the failure set where the vehicle remains controllable (e.g., the generation of thrust differentials to overcome a locked-in-place rudder).

Note that the LTI plants used for designing the nominal controller are good approximations of the aircraft dynamics as long as the longitudinal and lateral/directional dynamics are weakly coupled. However, for high angles of attack and for many adverse flying conditions this coupling is strong; e.g., when both left elevators are locked in place, any deflection of the right elevators will excite the lateral/directional dynamics. In this case, the adaptive component of the controller, which is based on a coupled model, will be active.

1. Reference Model

The reference model is a component of the adaptive controller responsible for setting the desired closed-loop dynamics. These target dynamics are the same for both nominal and offnominal flying conditions (e.g., those when physical failures and/or damage have occurred) regardless of the amount of control authority available. The reference model assumed herein is the linear closed-loop system corresponding to the nominal controller without antiwindup modifications under nominal flying conditions. This leads to:

$$\dot{x}_m = \underbrace{\left(\begin{bmatrix} A_p(\bar{p}) & 0 \\ H & 0 \end{bmatrix} + \begin{bmatrix} B_p \\ 0 \end{bmatrix} G_{\text{nom}} K_n \right)}_{A_m} x_m + B_m \hat{r} \quad (25)$$

where $A_m \in \mathbb{R}^{10 \times 10}$, $B_m \in \mathbb{R}^{10 \times 4}$,

$$x_m = [\alpha \quad \beta \quad V \quad p \quad q \quad r \quad e_\alpha \quad e_\beta \quad e_p \quad e_V]^\top$$

and

$$\hat{r} = [\alpha_{\text{cmd}} \quad V_{\text{cmd}} \quad \beta_{\text{cmd}} \quad p_{\text{cmd}}]^\top$$

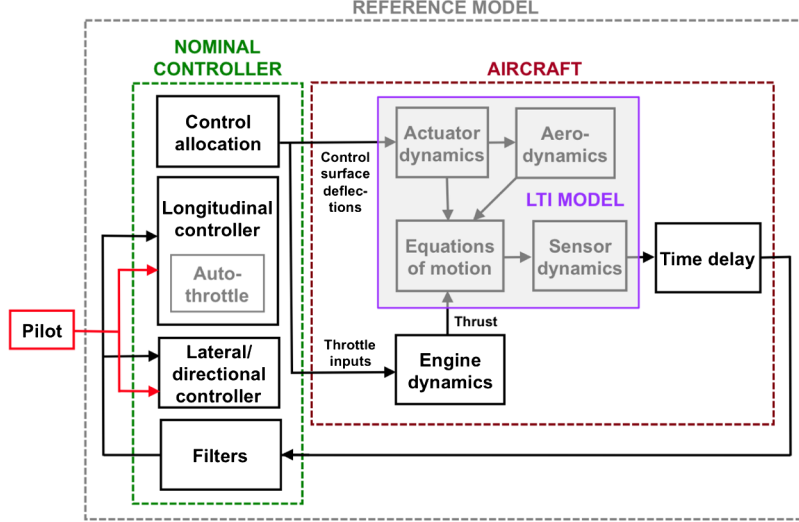


Fig. 3 Implemented reference model.

This model will be used to design the adaptive controller, but not for calculating x_m during implementation. Details of the reference model implementation are provided next.

The dynamics of the linear reference model in Eq. (25) may differ considerably from those of the actual aircraft. The unmodeled linear dynamics and nonlinearities responsible for this will trigger undesired adaptation. Since the primary objective of adaptive control is to compensate for parametric uncertainties and not for nonlinear dynamics,[§] this situation may seriously compromise the aircraft's stability and performance. In this section we examine alternatives for expanding the flight envelope where the reference model describes accurately the closed-loop dynamics corresponding to the nominal controller. A natural choice for the plant model in the reference model design is a full nonlinear model. Even though this will directly account for the main nonlinearities, the computational requirements associated with it may be exceedingly high. This complexity results from having to perform a high-fidelity simulation in real time, as well as from having to verify and validate software and hardware. The search for an accurate yet simple reference model led us to the system in Fig. 3. The main features of this system are as follows:

- 1) The underlying structure of the plant is LTI (see Sec. III.D for an exception to this statement).
- 2) There is an engine model to accurately describe the nonlinear dependency of the thrust on the engine's rpm.
- 3) There is uplink time delay between the controller and the plant capturing the effects of telemetry and signal processing.
- 4) There is a downlink time delay due to sensor dynamics.
- 5) There is a bank of low-pass filters for mitigating sensor noise.
- 6) There are anti-aliasing filters and command rate limiters as in the GTM.

The states of the reference model implemented include those in the reference model used for design, x_m , the altitude, the three Euler angles, all the delayed states and those of the engine dynamics. Note, however, that only those in x_m affect the adaptive controller. The sum of the time delay in items 3 and 4 constitute a known time delay. In particular, they account for a 9 ms downlink delay in all the states used for feedback and a 12 ms uplink delay in the application of the controller's output to the plant. Note that the implementation of this reference model is a significant departure of the LTI framework supporting the theory; i.e., signal boundedness and asymptotic tracking cannot be guaranteed theoretically.

[§]In general, the primary objective of adaptive control is to compensate for parametric uncertainties and unmodeled dynamics locally. The latter objective can be attained by identifying the coefficients of a radial basis function expansion of such dynamics. However, the effect of nonlinearities can not be perfectly compensated for globally. The controller proposed does not compensate for such nonlinearities.

2. Adaptive Law

In this section we present an adaptive law that accounts for control saturation and integration antiwindup. This antiwindup scheme is independent of the antiwindup scheme applied to the baseline controller.

The plant to be controlled assumes the LTI representation:

$$\dot{x} = \begin{bmatrix} A_p(\hat{p}) & 0 \\ H & 0 \end{bmatrix}x + B_1 \Lambda(\hat{p})(R_s(u) + d) + B_2 \hat{r} \quad (26)$$

where $A_p \in \mathbb{R}^{10 \times 10}$, $B_1 \in \mathbb{R}^{10 \times 5}$, $\Lambda = \text{diag}\{\lambda\} \in \mathbb{R}^{5 \times 5}$ and $B_2 \in \mathbb{R}^{10 \times 4}$. The states, inputs, and commands in Eq. (26) are

$$\begin{aligned} x &= [x_{\text{lon}}^\top \ x_{\text{lat}}^\top \ e_\alpha \ e_V \ e_\beta \ e_p]^\top \\ u &= [\delta_e \ \delta_a \ \delta_r \ \delta_{\text{thL}} \ \delta_{\text{thR}}]^\top \\ \hat{r} &= [\alpha_{\text{cmd}} \ V_{\text{cmd}} \ \beta_{\text{cmd}} \ p_{\text{cmd}}]^\top \end{aligned} \quad (27)$$

while $d \in \mathbb{R}^{5 \times 1}$ is a vector of input disturbances.

The preallocated adaptive input is given by

$$u_a = [\theta_x \ \theta_d] \begin{bmatrix} \hat{x} \\ 1 \end{bmatrix} = \theta^\top \omega \quad (28)$$

where $\theta_x \in \mathbb{R}^{5 \times 10}$ and $\theta_d \in \mathbb{R}^{5 \times 1}$ are adaptive parameters, and

$$\hat{x} = [x_{\text{lon}}^\top \ x_{\text{lat}}^\top \ f(e_\alpha) \ e_V \ e_\beta \ e_p]^\top \quad (29)$$

is the state being fed back. The function f , which is part of the adaptive antiwindup logic, is defined as $f(e_\alpha) = R_e(e_\alpha, \delta_e)$. Adaptive laws without the antiwindup modification make f equal to its argument so $\hat{x} = x$. The adaptive input is

$$u_{\text{ada}} = G_{\text{ada}} u_a \quad (30)$$

where $G_{\text{ada}} \in \mathbb{R}^{10 \times 5}$ is a control allocation matrix. The allocation of u_a by G_{ada} makes the deflection of the four elevators equal, the deflection of both rudders equal, and the deflection of both ailerons equal in magnitude with opposite directions.

The adaptive gains are given by [12]

$$\dot{\theta} = \text{Proj}\{-\Gamma_1 \omega e_u^\top P B_1 \text{sign}(\Lambda) \Gamma_2, \theta_{\max}\} \quad (31)$$

$$\dot{\lambda} = -\Gamma_\lambda \text{diag}(\kappa) B_1^\top P e_u \quad (32)$$

$$\dot{e}_\Delta = A_m e_\Delta - B_1 \text{diag}(\hat{\lambda}) \kappa \quad (33)$$

$$e_\Delta = u_\Delta + (K_{e_\alpha}^\top + \theta_{e_\alpha}^\top) e_{\alpha, \Delta} \quad (34)$$

where $\text{Proj}\{\cdot\}$ is the projection operator [13], $e_u = e - e_\Delta$, $P = P^\top > 0$ satisfies $A_m^\top P + PA_m = -Q$ for a fixed $Q = Q^\top > 0$, $e = x_p - x_m$, and u_Δ is the multivariable version of the input deficiency in Eq. (13). While e_Δ is the error caused by the saturation of the control inputs and of the integral error state e_α , e_u can be considered as the error caused by parametric uncertainties. The variables $Q > 0$, $\Gamma_1 \in \mathbb{R}^{11 \times 11} > 0$, $\Gamma_2 \in \mathbb{R}^{5 \times 5} > 0$, $\theta_{\max} \in \mathbb{R}^{11 \times 11} > 0$, and $\Gamma_\lambda \in \mathbb{R}^{5 \times 5} > 0$ are design parameters. Note that Γ_1^{-1} and Γ_2^{-1} are analogous to the state and control weighting matrices Q and R of an LQR setting. Γ_1 determines the rate of adaptation as a function of the state ω , whereas Γ_2 determines the rate of adaptation as a function of the control inputs. Rates of adaptation for states and inputs are inversely proportional to the Q and R penalty matrices.

The *antiwindup modification* to the adaptive law is enforced using the variable κ , which depends on the column vectors of K_n and θ corresponding to $R_e(e_\alpha, \delta_e)$ and $f(e_\alpha)$, respectively. In contrast to the antiwindup modification of Sec. II.C.1, this antiwindup modification not only modifies the integral error state used for feedback (i.e., ω), but also changes the controller gain (i.e., θ). The antiwindup modification for the (e_α, δ_e) pair is based on monitoring the total elevator input and modifying the integral error state of the adaptive controller when saturation occurs. The strong coupling between β and p , and the nonlinear engine dynamics made the antiwindup modification for the (e_β, δ_a) , (e_p, δ_r) , and (e_V, δ_{th}) pairs ineffective. This is the reason κ in Eq. (34) only takes e_α into account. The modifications for the (e_V, δ_{th}) , (e_β, δ_r) , and (e_p, δ_a) pairs, which are solely based on the developments of Sec. II.C.1, are based on monitoring the control inputs generated by the nominal controller and modifying the integral error states of such a controller when saturation/desaturation occur.

Note that the integral error states depend on the command \hat{r} , but the error e_u driving adaptation does not. The adaptive controller achieves command tracking by making x_p follow x_m via the adaptive law, and by making $x_m \rightarrow 0$ via a stable reference model (i.e., if $x_p \rightarrow x_m \rightarrow 0$ then the plant states $[\alpha, V, \beta, p]$ approach the pilot commands \hat{r}). If saturation occurs e will be bounded and x_p will not necessarily converge to x_m .

The adaptive law in Eqs. (31–34) makes the plant's state track the state of the reference model, accommodates for control saturation, and mitigates the effects of integral windup in e_α . The Lyapunov stability analysis in [12] demonstrates that for a bounded set of commands, θ , x , and e are semiglobally bounded. This result holds under the assumption that the disturbances, time delays, and unmodeled dynamics are not present and that both the plant and the reference model are LTI.

In the LTI framework supporting the theory, asymptotic tracking and stability are guaranteed for any adaptation rates satisfying $\Gamma_1 > 0$, $\Gamma_2 > 0$, and $\Gamma_\lambda > 0$. While excessively small adaptation rates nullify the advantages of adaptation by practically turning the adaptive controller off, excessively large ones, along with noise, saturation, time delay, and/or unmodeled dynamics, induce high-frequency oscillations that may not only degrade the system performance, but also lead to instability. The challenge from the control designer perspective is to balance these two attributes. A dead zone, where Γ_1 and Γ_λ are made equal to zero (i.e., adaptation is switched off), depending on the state of the aircraft x_p , the pilot's command \hat{r} , and the tracking error due to uncertainties e_u , can be used to counteract some of the anomalies caused by unmodeled dynamics. In particular, we imposed dead zones when the deviation in V and bank angle from the trim state were large. In those regions, the significant discrepancies between the dynamics of the reference model and of the plant trigger adaptation unintentionally. The domain where the adaptive rates are nonzero, and $\theta < \theta_{\max}$ in Eq. (31) defines the range of adaptation.

III. Simulation Studies

In this section we showcase some of the advantages and disadvantages of adaptation using a set of batch simulations for various realizations of the uncertainty/failure. These are simulations where the reference commands are set a priori and for which the

aircraft performs the desired maneuver under nominal flying conditions. For this we use the high-fidelity model described in Sec. I, a set of representative flying maneuvers, a flight-validated nominal controller [14] (see Sec. VI.B for some details on the validation process), and adaptive controllers with the structure as above but having various adaptation rates. These rates were prescribed according to the observed aircraft performance for a representative set of flying maneuvers and uncertainties among an extensive set of candidate designs. This is the most conventional tuning practice.

A. Tradeoffs

Figure 4 shows the closed-loop response of the nominal and augmented controllers to a set of command doublets when the effectiveness of the elevators is reduced to 50% and a severe degradation in pitch stiffness C_{mo} and roll damping C_{lp} occur. This case corresponds to 100% uncertainty in the nominal value of the aerocoefficients (open-loop marginal stability). Note that the nominal controller is unable to stabilize the pitch dynamics. The augmented controller on the other hand, not only stabilizes these dynamics, but also exhibits a much better roll rate tracking. This is a situation where adaptation yields a significant improvement in performance.

Unfortunately, the adaptive component of this controller is overly aggressive for other types of uncertainties. Figure 5 shows the closed-loop response for the same controllers when there is an uplink time delay of 60 ms. While the nominal controller achieves command tracking with minimal residual oscillations, the augmented controller yields a severely degraded response. The response to larger time delays, where the nominal system response is stable but the augmented one is not, demonstrates that adaptation itself can compromise safety. The cases above highlight the importance of prescribing adaptive rates that effectively compensate for uncertainties and failures without magnifying the adverse effects caused by unmodeled dynamics and time delays.

B. Unrealizable Reference Model Dynamics

It is important to determine if the reference model prescribes dynamics that the aircraft is able to realize (even in the case where the aircraft remains controllable after a failure). If physical limitations prevent the aircraft from attaining the dynamics set by the reference model -for example due to failure, damage or uncertainty- the controller itself, and thereby the plant, will become unstable. This instability, which is triggered by the adaptive component of the controller, can be avoided if a more suitable reference model is used. Figure 6 shows the augmented closed-loop response when a flawed

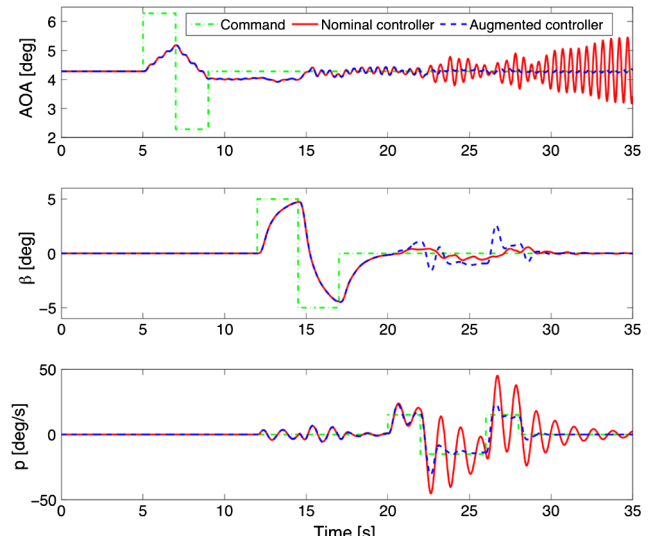


Fig. 4 Closed-loop responses corresponding to the nominal and augmented controllers.

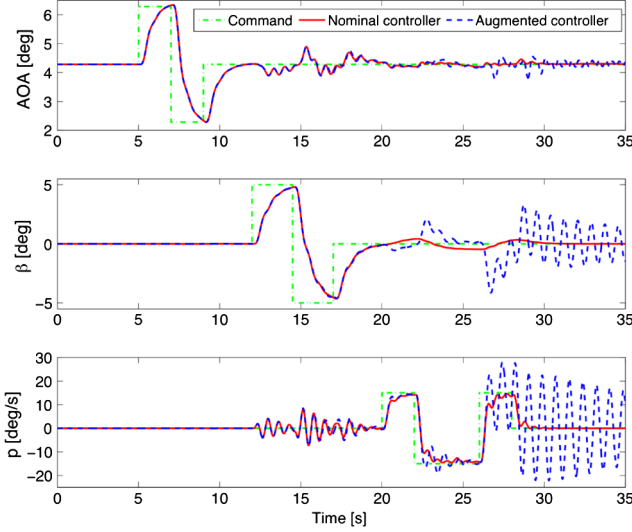


Fig. 5 Closed-loop responses corresponding to the nominal and augmented controllers.

reference model is used. This model uses a low-pass filter whose bandwidth is 2 Hz off from that of the actual telemetry of the aircraft. No uncertainty or failure occurs.

In this simulation, periodic wave trains for α_{cmd} and p_{cmd} are used to aggravate the effects of the mismatch. Note that as time goes on, the ability of the controller to track the reference model worsens progressively. This progression, which makes the integral error states of the adaptive component grow, will eventually lead to instability.

Note that the adaptive controller will react to any error between the dynamics of the aircraft and the dynamics of the reference model regardless of its origin. This error may be caused by disturbances, time delays, unmodeled dynamics, matched parametric uncertainties (i.e., uncertainties satisfying the matching conditions for which the adaptive controller has been designed for) or unmatched parametric uncertainties (i.e., uncertainties that do not satisfy the matching conditions and for which the controller can only be robust). Although the adaptation (i.e., change in the adaptive gains θ) triggered by matched uncertainties is desirable, adaptation to all other causal factors is not. The existence of unmatched uncertainty will appear to the controller as a disturbance. If this disturbance is large, the controller, thus, the plant may become unstable. The outcome resulting from unmatched uncertainty cannot be predicted theoretically. This observation holds for all model reference adaptive architectures requiring the existence of matching conditions. Dead zones can be

used to prevent the error from triggering adaptation. The key aspect of designing these zones is determining where to apply them (i.e., the region in the state, error and input spaces where adaptation will be switched off). This determination requires knowledge of the region in the flight envelope where the reference model accurately represents the aircraft dynamics. Efforts aiming at evaluating and expanding this region would be beneficial.

C. Actuator Anomalies: Surface Deadband

Figure 7 shows the effects of control surface deadband on the same augmented controller used in Fig. 4 for the same uncertainty/failure realization. Even though asymptotic tracking is ultimately achieved, the significant degradation in the transient response makes the controller unacceptable. It is worth highlighting that the effects of this actuator anomaly on the nominal controller (not shown) are barely noticeable. In practice, the nonlinear effects of anomalies like this one (e.g., hysteresis) are a function of the aircraft's state and, as such, strategies based on their offline inversion may not be effective. Since the aircraft is uncontrollable within the surface deadband, the tracking error cannot be driven to zero. Consequently, small tracking residues will build up in the integral error states over time. When these states are sufficiently large, they will make the input u large enough to make the control surface leave the deadband. Outside of the band the control surfaces are effective again, and the controller will drive the surface deflections back into the deadband. This chattering cycle will keep repeating unless an adaptive dead zone is applied. This zone will diminish the controller's ability to compensate for parametric uncertainty, however. Better strategies can be applied if measurements of the control surface deflections are available. The chattering can be eliminated by removing the effects of the actuator anomalies from the adaptive law, i.e., by using $u_\Delta = u - u_{\text{measured}}$ in Eq. (34). This was the strategy implemented.

D. Knowing the Sign of Λ

There are physical effects for which a single LTI system cannot capture the aircraft dynamics accurately regardless of the proximity of the state to the equilibrium point used for linearization. For instance, the loss in altitude caused by either a positive or a negative aileron deflection cannot be modeled with a fixed input matrix B . A fixed B matrix leads to a situation where rolling to one side will decrease altitude while rolling to the other one will increase it. The physics of this phenomenon are better modeled as $B|u|$. Even though this is a second-order effect in the coupling between the longitudinal and lateral/directional dynamics, it has the potential to make the reference model dynamics unrealizable and therefore to make the system unstable.

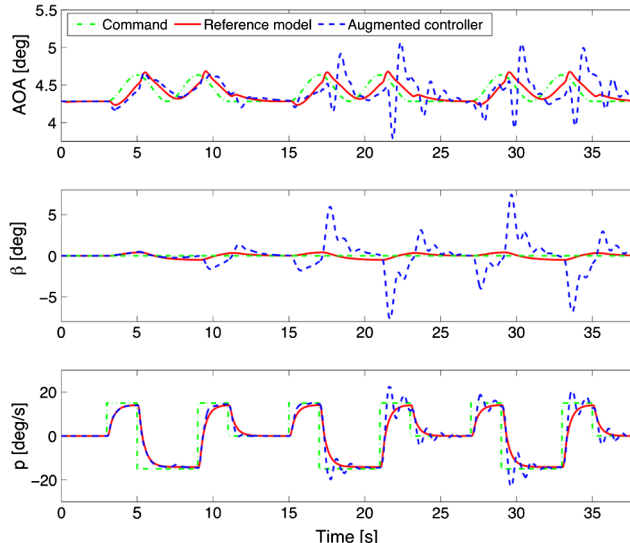


Fig. 6 Effects of unrealizable reference model dynamics.

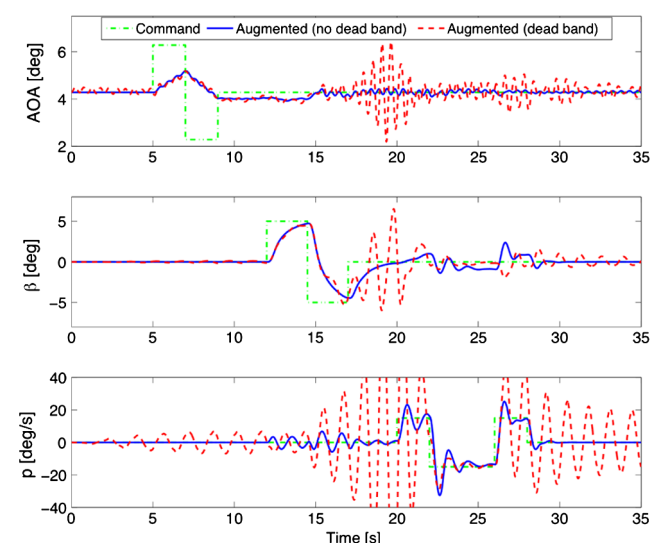


Fig. 7 Effects of deadband in control surfaces.

Note that from the perspective of the adaptive controller this is equivalent to not knowing the signs of the entries of Λ in Eq. (31). To prevent these difficulties, the sign of some of the components of the B_1 matrix in Eqs. (31–33) and in the reference model are switched according to the instantaneous value of the input. Figure 8 illustrates the consequences of using a fixed input matrix B when a periodic train of roll rate doublets is commanded. The same type of “buildup” behavior observed in Fig. 6 occurs. Note that the peaks in the angle of attack and progressively larger variations in velocity caused by the loss in altitude are absent from the dynamics of the reference model. In its attempt to make the falling aircraft respond as if it were a wings-level flight, adaptation ends up creating a large phase difference between the velocities of the aircraft and of the reference model. This phenomenon makes the integral error state of the controller e_V to grow unbounded and the adaptive component to become unstable.

E. Counteracting Actuation

The control inputs generated by the adaptive controller are independent signals. If some of these inputs correspond to actuators with similar functions (e.g., there is an input for each of the two rudder segments), the controller will perform control design and control allocation simultaneously. This independence may lead to situations where the inputs counteract. For instance, a situation may arise where the upper and lower rudders deflect in opposite directions so their overall effect on the yaw dynamics is nil. Even though this configuration may be able to achieve asymptotic tracking, the incidental increase in drag and fuel consumption makes the controller unacceptable. The simplest way to avoid this outcome is to restrict the adaptive controller to use nonredundant inputs. The resulting controller outputs will then be allocated using traditional control allocation methods. However, this practice eliminates degrees of freedom that the adaptive controller could take advantage of (e.g., the differential use of elevators may be able to compensate for aileron failures).

The point simulations above give an indication of the benefits and potential drawbacks of adaptation from a local perspective. The developments that follow aim at making this determination from a global perspective.

IV. Mathematical Framework for Robustness Analysis and Control Tuning

A. Robustness Analysis

A brief introduction to the methodology proposed in [9] is presented next. Consider the closed-loop dynamic system

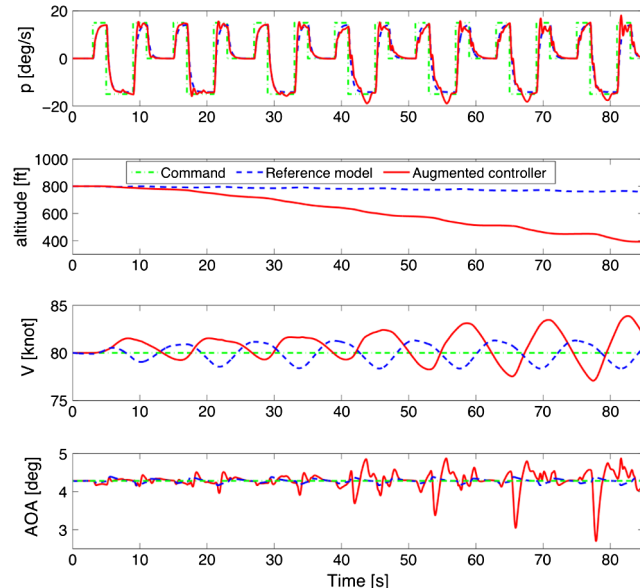


Fig. 8 Growing offset between LTI reference model and nonlinear plant.

$$\dot{x} = f(t, x, \hat{p}, u, \hat{r}) \quad (35)$$

The control input can be represented as

$$u = U(t, x, \hat{r}, k) \quad (36)$$

where the function U refers to a particular control structure and $k \in \mathbb{R}^{\dim(k)}$ is the set of free parameters, to be chosen by the control engineer (e.g., control gains, adaptive rates), that fully prescribe the controller. The controller is deemed acceptable if the closed-loop response satisfies a set of requirements. These requirements, which are represented by a set of inequality constraints on selected output metrics, depend on the uncertain parameter vector \hat{p} . The control system is deemed acceptable if all inequalities are satisfied. Specifically, the satisfaction of the vector inequality

$$g(\hat{p}, \hat{r}, k) < 0 \quad (37)$$

where $g \in \mathbb{R}^{\dim(g)}$ implies the satisfaction of all the requirements.[†] For a fixed value of k and a fixed $r(t)$, these constraints partition the uncertain parameter space into two sets, the failure domain $F = \{\hat{p}: g(\hat{p}) \geq 0\}$, where at least one requirement is violated, and the safe domain $S = \{\hat{p}: g(\hat{p}) < 0\}$, where all requirements are satisfied. The term *satisfactory performance*, which is to be captured in g , is broad in scope and refers to acceptable ranges of variation in metrics of interest. These metrics may correspond to specific performance specifications, as well as to commonsensical notions of goodness. For instance, if $y(\hat{p}, t)$ is the system output to a step input, t_{ar} is the admissible rise time, t_{as} is the admissible settling time, and M_{ap} is the admissible percent overshoot; requirement functions corresponding to these requirements are $g_{rise} = t_r - t_{ar}$, where t_r satisfies $y(\hat{p}, t_r) = 0.9$; $g_{settling} = t_s - t_{as}$, where t_s is given by $|y(\hat{p}, t) - y(\bar{p}, \infty)| \leq 0.99$ for all $t > t_s$; and $g_{overshoot} = M_p - M_{ap}$, where $M_p = \max_t \{y(\hat{p}, t) - y(\bar{p}, \infty)\}$.

Let $\bar{p} \in \mathbb{R}^{\dim(\bar{p})}$, called the nominal operating conditions point, denote our best estimate of the actual value of \hat{p} . The objective of this robustness analysis is to determine the largest deviation from \bar{p} for which all the requirements are met. In this paper, such a deviation will be prescribed as a hyperrectangular set of fixed proportions. Note that the hyperrectangle centered at \bar{p} with aspect vector $m > 0$ is given by

$$R(\bar{p}, m) = \{\hat{p}: \bar{p} - m \leq \hat{p} \leq \bar{p} + m\} \quad (38)$$

The notions required to calculate this deviation are introduced next.

A *homothetic* deformation results from a uniform, radial expansion or contraction of the space about a fixed point. The distance from any point in the space to the fixed point changes by a factor ε after the deformation. This factor is called the *similitude ratio* of the homothetic deformation. Note that if ε is greater than 1, the deformation is an expansion, while if ε is less than 1, the deformation is a contraction. A reference set, denoted as $\Omega \subset \mathbb{R}^{\dim(\bar{p})}$, will be deformed with respect to its geometric center \bar{p} . Intuitively, one can imagine that Ω is being deformed with respect to $\bar{p} \in S$ until its boundary just touches the failure-domain boundary ∂F . This deformation will be called the *maximal deformation*. The set resulting from this deformation, denoted as $M \subseteq \mathbb{R}^{\dim(\bar{p})}$, is the maximal set. A critical parameter value (CPV), denoted as $\tilde{p} \in \mathbb{R}^{\dim(\bar{p})}$, is (one of) the point(s) where the maximal set touches ∂F . This point is the worst-case uncertainty combination associated with Ω . The critical similitude ratio (CSR), denoted by $\tilde{\varepsilon} \in \mathbb{R}$, is the similitude ratio of that deformation and is a nondimensional metric proportional to the separation between the point \bar{p} and the failure domain. The parametric safety margin (PSM), denoted as $\rho \in \mathbb{R}$ is its dimensional equivalent. The values taken on by the CSR and the PSM are proportional to the size of the maximal set and measure the separation between \bar{p} and F . In regard to measuring this separation;

[†]For the remainder of the paper it is assumed that vector inequalities hold componentwise, vector and set superindices denote a particular realization, and vector subindices denote a particular component; e.g., p_i^j is the i th component of $p^j \in \mathbb{R}^{\dim(p)}$.

the approach is exact; i.e., there is no conservatism. If the PSM takes on a negative value, the controller does not even satisfy the requirements at \bar{p} . In such a case, the deformation is done until the deformed set touches F . If the PSM is zero, the controller exhibits no robustness because there is an arbitrarily small deviation from \bar{p} leading to a requirement violation. If the PSM is positive, the requirements are satisfied at \bar{p} and its vicinity. The larger the PSM, the larger the Ω -shaped vicinity where the requirements are satisfied.

Figure 9 illustrates some of these variables when two requirements are present. The CPV \tilde{p} , the nominal parameter point \bar{p} , the reference set (region within dashed line), and the maximal set corresponding to deformations in the safe and failure domains are shown. Note that by construction, the maximal set is fully contained in the safe or failure domains.

The formulation enabling sizing the maximal deformation is as follows. If $\Omega = R(\bar{p}, m)$, the CPV, CSR, PSM, and maximal sets corresponding to the i th requirement are

$$\tilde{p}^i = \arg \min_{\hat{p}} \{\|\hat{p} - \bar{p}\|_m^\infty : \sigma_i g_i(\hat{p}, \hat{r}, k) \geq 0, \hat{p}_{\min} \leq \hat{p} \leq \hat{p}_{\max}\} \quad (39)$$

$$\tilde{\varepsilon}_i = \frac{\|\tilde{p}^i - \bar{p}\|_m^\infty}{\|m\|} \quad (40)$$

$$\rho_i = \sigma_i \tilde{\varepsilon}_i \|m\| \quad (41)$$

$$M^i = R(\bar{p}, \tilde{\varepsilon}_i m) \quad (42)$$

where $\|x\|_m^\infty = \max_i \{|x_i|/m_i\}$, \hat{p}_{\min} and \hat{p}_{\max} bound the region of interest, and $\sigma_i = 1$ if $g_i(\bar{p}) < 0$; otherwise, $\sigma_i = -1$. The value of the controller's parameters k and the commands in \hat{r} are set a priori and kept fixed during the analysis. Whereas k can be prescribed according to any control design practice, \hat{r} should yield a representative set of flying maneuvers when $\hat{p} = \bar{p}$.

The CPV, CSR, PSM, and maximal sets associated with all requirements are given by Eqs. (39–42) after replacing g_i with $\max_i(g_i)$. The resulting values, to be qualified as *aggregate*, since they take all requirements into account, coincide with those corresponding to the individual requirement attaining the smallest PSM, e.g., $\tilde{\varepsilon} = \tilde{\varepsilon}_j$, where $j = \arg \min(\rho_i)$. Therefore, the aggregate PSM is the worst-case individual PSM.

The calculation of the maximal deformation requires solving a standard optimization problem. Such a problem is nonconvex when the dependency of the requirement functions g on the uncertainty \hat{p} is nonlinear. In any nonconvex optimization problem there is always the possibility of convergence to a nonglobal optimum. When this occurs, the CPV resulting from the numerical optimization is mistaken and the corresponding maximal set intrudes into the failure region. This intrusion yields to a spuriously larger PSM. Absolute guarantees are not possible, but a variety of algorithmic safeguards

can be used to deal with this deficiency. For instance, g can be evaluated at a few sample points in the maximal set and if one happens to fall into the failure domain, it can be used as an initial condition in a subsequent optimization. Requirements functions with a polynomial parameter dependency can be handled using the methods in [15]. These methods, which are based on linear matrix inequalities and Bernstein expansions, will not suffer from this potential drawback and will guarantee convergence to actual maximal deformation. Note, however, that in most practical applications the explicit functional form of g is unknown. This intrinsic feature of the problem precludes the usage of convexity conditions from the outset.

B. Control Tuning

Ultimately, a good controller should satisfy the stability and performance requirements imposed upon the closed-loop system with sufficiently large robustness margins. The PSM and CSR introduced above are examples of such margins. A computational framework that enables searching for the set of controller gains that maximize these margins is introduced next.

Equation (37) indicates that the geometry of the failure domain, thus the CSR and the PSM, is a function of the control parameter k . Recall that this parameter is kept fixed when a robustness analysis is performed. A control design challenge is to find the value of k for which the closed-loop system exhibits satisfactory robustness characteristics. The design points targeted subsequently realize the largest overall PSM the control structure U allows for. This entails maximizing the separation between the nominal operating condition point \bar{p} and the failure domain F , so the largest maximal set is attained. Since the resulting controllers tolerate the largest deviations from nominal operating conditions before violating any requirement, they will be called *optimally robust*. In the presence of conflicting design objectives, an optimally robust controller trades off the PSM of all individual requirements to attain the largest aggregate PSM.

Two optimization-based formulations for pursuing the optimally robust design point \tilde{k} are presented next. The first one evaluates robustness via the exact CSR. The second one uses an approximation to the CSR rooted in a multipoint approximation to the maximal set. The approximate nature of this formulation may not lead to controllers with the intended features. However, its relaxed computational demands may justify the potential drawbacks associated with it.

1. Enlarging the Maximal Set

A formulation based on the exact overall CSR is given by

$$\tilde{k} = \arg \max_k \{\tilde{\varepsilon}(k) : h(k, \bar{p}) > 0\} \quad (43)$$

where the vector constraint $h(k, \bar{p}) > 0$ is used to enforce additional characteristics to the controller based on standard control metrics. For instance, $h = PM(k, \bar{p}) - 60^\circ > 0$ ensures that the feedback loop corresponding to the plant under nominal operating conditions has a phase margin of more than 60 deg. Examples of other performance/stability metrics are time delay, settling time, disturbance rejection, noise attenuation, reference tracking, and control energy. These metrics can be extracted from the time and/or frequency domains and may correspond to linear and nonlinear representations of the plant dynamics.

Recall that calculating the CSR $\tilde{\varepsilon}$ entails solving an optimization problem. Therefore, this formulation has an optimization in the outer loop and another 1 in the inner loop. While the outer loop searches for the robustly optimal gains \tilde{k} , the inner one searches for the CSR corresponding to the design point under consideration. Nested optimizations, such as Eq. (43) and those resulting from worst-case-based design policies, impose stringent computational demands. Such demands can be substantially mitigated by using multipoint approximations.

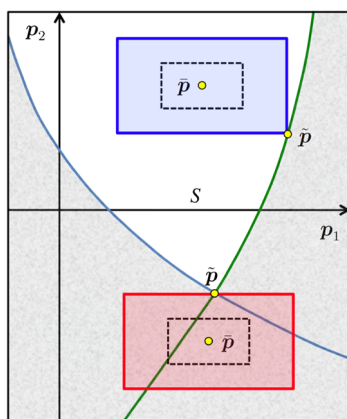


Fig. 9 Maximal deformations in the safe and failure domains.

2. Enlarging an Approximation to the Maximal Set

The variables \hat{k} and $\hat{\varepsilon}$, which are estimates of \tilde{k} and $\tilde{\varepsilon}(\tilde{k})$, respectively, are given by

$$\begin{aligned} \{\hat{k}, \hat{\varepsilon}\} &= \arg \max_{k, \varepsilon} \{ \varepsilon : \max_{i \leq \dim(g), j \leq n} \{ g_i(\bar{p} + \varepsilon(p^j - \bar{p}), \hat{r}, k) \} < 0, \varepsilon \\ &\geq 0, h(k, \bar{p}) > 0 \} \end{aligned} \quad (44)$$

where $\{p^1, p^2, \dots, p^n\}$ are parameter points on the surface of $R(\bar{p}, m)$. These points, which only have to be computed once [16], should be uniformly distributed over the surface. Note that this formulation replaces the inner optimization loop in Eq. (43) with a multipoint constraint over parameter points lying on the surface of a maximal-set estimate. Equation (44) may lead to suboptimal designs, for which $\hat{\varepsilon} > \tilde{\varepsilon}(\tilde{k})$ and $M(\hat{k}) \subset M(\tilde{k})$, because the satisfaction of the multipoint constraint does not guarantee the containment of the maximal-set estimate by the safe domain. The formulation of Sec. IV.A can be used to determine if this anomaly has occurred.

Since the robustness analysis and tuning procedures above identify the critical combination of uncertainties and/or failures (i.e., the CPV) the particular control architecture is more sensitive to, we expect the resulting controllers to be *safer* than those validated by brute force Monte Carlo simulations.

C. Application to the GTM

The components of the uncertain parameter \hat{p} can be grouped into four categories: actuator failures, unknown time delays, structural damage, and aerodynamic uncertainties. Details of the particular components comprising p are provided next.

The parameters Λ_{THL} , Λ_{THR} , Λ_{ERO} , Λ_{ERI} , Λ_{ELO} , Λ_{ELI} , Λ_{AL} , Λ_{AR} , Λ_{RU} , and Λ_{RD} are the control effectiveness of the main 10 inputs [17]. These are the throttle input to the left and right engines, the four elevators, the left and right ailerons, and the upper and lower rudders. These parameters, which are used to describe both loss in control effectiveness and locked-in-place failures, should be interpreted as follows: If $0 < \Lambda \leq 1$ the actuator will suffer a loss in control effectiveness, making the actual plant's input $R_s(\Lambda u + U_0)$. If $-1 \leq \Lambda \leq 0$, the actuator will be locked from the time of the failure at $\Lambda(U_{\max} - U_0) + U_0$.

Moreover, $\tau > 0$ is an unknown uplink time delay. This is an additional time delay to the known time delay specified in Sec. II.C.1. $\mu > 0$ is a scaling factor proportional to the amplitude of the doublet commands in \hat{r} , and Δ_x and Δ_y are displacements of the c.g. from its nominal location due to structural damage. The value of Δ_x will be specified as a percentage of the mean aerodynamic chord. In addition, its sign is consistent with the orientation of the body axes; e.g., $\Delta_x = -0.5$ implies an aft shift in the c.g. location equal to 50% of the mean aerodynamic chord.

Furthermore, δC_{ma} , δC_{lp} , and δC_{nr} are aerodynamic uncertainties in pitch stiffness, roll damping, and yaw damping. These uncertainties are enforced in both the high-fidelity simulation and the test article by manipulating primary and secondary control surfaces against the actions commanded by the flight control system. Auxiliary feedback loops, aimed at artificially degrading the nominal stability derivatives were designed by NASA Langley. In particular, δC_{ma} was generated by taking the inner elevators out of the flight control loop ($\Lambda_{\text{ERI}} = \Lambda_{\text{ELI}} = 0$) and using an auxiliary control loop to make the inner elevators counteract the actions of the outer ones. The bigger the counteraction, the larger the effective value of δC_{ma} . Similarly, δC_{nr} was enforced by taking the lower rudder out of the flight controller ($\Lambda_{\text{RD}} = 0$) and making it counteract the actions of the upper one. δC_{lp} was generated by making the spoilers counteract the ailerons ($\Lambda_{\text{AL}} = \Lambda_{\text{AR}} = 1$). This setting enables evaluating the robustness of the controller to these aerodynamic uncertainties in both the high-fidelity simulation and the flight experiment.

The maneuver generated by \hat{r} consists of a sequence of doublets in α_{cmd} , β_{cmd} and p_{cmd} . When $\mu = 0$ the commands keep the vehicle trimmed at the point used for control design. As μ increases, the commands make the vehicle depart from this trim point. The

amplitude of the doublets is proportional to the value of μ . The commands in Fig. 4 correspond to $\mu = 1$. The larger the value of μ , the larger this departure and the larger the second-order effects absent in the LTI plant model. By including μ into \hat{p} , we evaluate the sensitivity of the response to such effects.

The flight condition corresponding to the nominal operating condition point \bar{p} is 1 in, which $\mu = 1$, the actuators are fully functional (i.e., effectiveness of all actuators is one), there is no additional time delay in the processing and communication of signals, the c.g. remains at its nominal location and there are no aerodynamic uncertainties.

The closed-loop requirements defining the constraint function g , whose functional forms are given in [11], are as follows:

1) The satisfaction of $g_1 < 0$, describing the *structural loading* requirement, ensures that the loading factor caused by the vehicle's acceleration does not exceed the structural stress limit.

2) The satisfaction of $g_i < 0$ for $i = 2, 3, 4, 5$, describing the *command tracking* requirements, ensures that the aircraft satisfactorily tracks the pilot commands α_{cmd} , β_{cmd} , V_{cmd} , and p_{cmd} , respectively: i.e., that the L_2 norm of the difference between the command and the corresponding state is bounded.

3) The satisfaction of $g_6 < 0$, describing the *safe flight envelope* requirement, ensures that the vehicle's state remains within a safe flight envelope throughout the maneuver. This envelope is prescribed by $-5 \text{ deg} < \alpha < 30 \text{ deg}$, $-20 \text{ deg} < \beta < 20 \text{ deg}$, $50 \text{ kt} < V < 110 \text{ kt}$, $-90 \text{ deg/s} < p, q, r < 90 \text{ deg/s}$, and $0 \text{ ft} < h < 1200 \text{ ft}$.

4) The satisfaction of $g_7 < 0$, describing the *ride quality and high-frequency oscillation* requirement, ensures that the amount of energy in the high-frequency part of the power spectrum of the response is bounded. For this application, frequencies above 2 Hz are regarded as high. This limit, which is set according to the pilot's opinion on the time scale the aircraft can be easily maneuvered, is well below the first natural frequency of the structure, which is 16 Hz. The separation between the time scales of the adaptation process and of the closed-loop dynamics [18] is addressed indirectly. The time scale of the adaptation law is proportional to the adaptive rates Γ_1 , Γ_2 and Γ_λ . Excessively large adaptive rates, for which the separation is small, yield poor transient responses having a power spectra with a sizeable high-frequency content. These responses violate the requirement $g_7 < 0$. Therefore, we are enforcing time-scale separation by using $g_7 < 0$ in the control tuning procedure.

5) The satisfaction of $g_i < 0$ for $i = 8, 9$, describing the *reference tracking* requirement, ensures that the offset between the pitch rate and roll rate of the plant and reference model is bounded.

The constraint functions corresponding to all tracking requirements are evaluated using the L_2 norm of aircraft states; therefore, they are a function of the transient response. Note that the dependency of g on \hat{p} assumes an unknown and implicit functional form. Also note that evaluating g for a particular realization of \hat{p} requires simulating the closed-loop response and calculating the nine constraint functions comprising g . Further note that while the notions of goodness supporting the requirement functions are fairly universal, their particular functional form is not. It is up to the analyst to construct functions that capture the intent of the vehicle's design specifications properly.

In this study the values of \hat{p}_{\min} and \hat{p}_{\max} , which prescribe the range of uncertainties of interest, are given by $-1 \leq \Lambda \leq 1$, $0 \leq \tau \leq 0.07$, $0 \leq \mu \leq 3$, $-0.5 \leq \Delta_x \leq 1$, $0 \leq \delta C_{lp} \leq 1$, $0 \leq \delta C_{ma} \leq 1$ and $0 \leq \delta C_{nr} \leq 1$. While the lower limit of the aerodynamic uncertainties indicates no aerodynamic degradation, the upper limit corresponds to perturbations of 125% from nominal values, with 100% being the point corresponding to neutral instability.

In designing the controller it is assumed that only matched uncertainties occur. However, there may be parametric uncertainties for which the matching conditions do not hold. While the objective of the robustness analysis framework is to evaluate the robustness to uncertainties the adaptive architecture may not have been designed for, the objective of the control tuning procedure is to improve the robustness to such uncertainties.

Table 1 One-dimensional PSMs for $U_{\text{nom}}(k_{\text{base}})$

	ρ_1	ρ_2	ρ_3	ρ_4	ρ_5	ρ_6	ρ_7	ρ_8	ρ_9
$\hat{p} = \Lambda_{\text{THL}}$	2.00	2.00	2.00	2.00	1.87	1.55	2.00	1.92	1.47
$\hat{p} = \Lambda_{\text{ELO}}$	2.00	2.00	2.00	2.00	1.50	2.00	2.00	2.00	1.67
$\hat{p} = \Lambda_{\text{AL}}$	2.00	2.00	2.00	1.81	1.30	1.72	1.75	1.87	1.24
$\hat{p} = \Lambda_{\text{RU}}$	2.00	2.00	2.00	2.00	2.00	2.00	2.00	2.00	1.27
$\hat{p} = \tau$	0.07	0.07	0.07	0.07	0.07	0.07	0.07	0.07	0.07
$\hat{p} = \mu$	2.00	2.00	2.00	2.00	2.00	1.16	2.00	2.00	2.00
$\hat{p} = \Delta_x$	0.46	0.28	0.46	0.42	0.17	0.12	0.31	0.29	0.42
$\hat{p} = \delta C_{lp}$	1.00	0.66	1.00	0.53	0.65	0.66	0.43	1.00	0.72
$\hat{p} = \delta C_{ma}$	1.00	0.79	1.00	1.00	1.00	1.00	0.76	0.77	1.00
$\hat{p} = \delta C_{nr}$	1.00	0.89	0.86	0.80	1.00	1.00	0.82	0.90	0.73

Table 2 Multidimensional PSMs and failure probabilities for $U_{\text{nom}}(k_{\text{base}})$

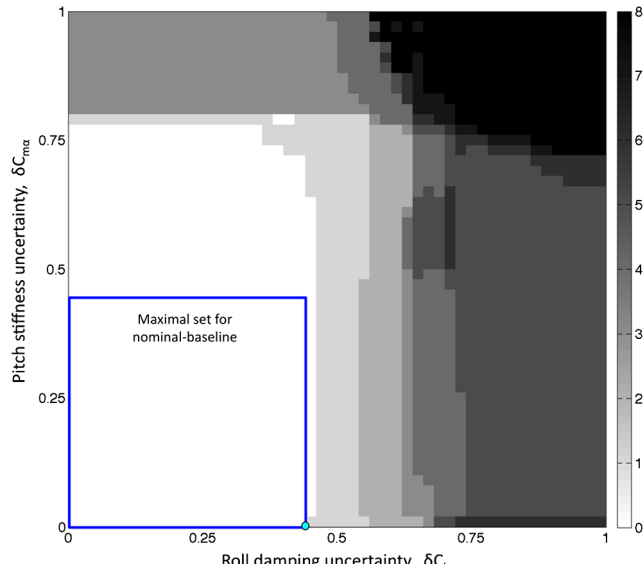
	ρ	$P[F]$
$\hat{p} = [\tau, \mu]$	2.1	7.5e - 2
$\hat{p} = [\delta C_{lp}, \delta C_{ma}]$	0.63	3.6e - 1
$\hat{p} = [\Delta_x, \Delta_y]$	0.095	7.7e - 1
$\hat{p} = [\tau, \delta C_{lp}]$	0.39	3.3e - 1
$\hat{p} = [\tau, \delta C_{ma}]$	0.52	1.2e - 1
$\hat{p} = [\tau, \delta C_{nr}]$	0.67	8.5e - 2
$\hat{p} = [\delta C_{lp}, \delta C_{nr}]$	0.59	3.7e - 1
$\hat{p} = [\Lambda_{\text{THR}}, \Lambda_{\text{RU,RL}}]$	1.08	4.5e - 2
$\hat{p} = [\tau, \eta]$	0.39	3.8e - 1
$\hat{p} = [\Lambda_{\text{ELO}}, \Lambda_{\text{ELI}}]$	1.59	1.5e - 2
$\hat{p} = [\tau, \delta C_{lp}, \delta C_{ma}, \delta C_{nr}]$	0.64	5.6e - 1
$\hat{p} = [\Lambda_{\text{THR}}, \dots, \Lambda_{\text{RD}}] \in \mathbb{R}^{10}$	1.68	2.4e - 1

V. Nominal Controller

This section presents the robustness analysis of the nominal controller for two sets of controller parameters. The corresponding control structure, to be denoted U_{nom} , requires removing the adaptive loop from the augmented architecture (i.e., $u = u_{\text{nom}}$). The analysis of the full augmented controller is presented in the section that follows. The comparison of these two analyses enables determining the merits of adaptation.

A. Nominal-Baseline Controller

The nominal-baseline controller will be denoted as $U_{\text{nom}}(k_{\text{base}})$. The gains of this controller were chosen based on classical margins of

**Fig. 10** Maximal set and failure and safe domains for $U_{\text{nom}}(k_{\text{base}})$.

stability and performance, as well as on the pilot's feedback. After several rounds of tuning and exhaustive testing in the simulator, we obtained a controller suitable for flight. Since the pilot's determination of whether a controller is suitable for flight or not mostly depends on testing under nominal flying conditions (i.e., $p = \bar{p}$), the acceptance or rejection of any given controller is independent of its robustness to parametric uncertainties. The maximal deformations of Sec. IV.A corresponding to several one-dimensional \hat{p} for each of the nine closed-loop requirements in Sec. IV.C were carried out. In these robustness analyses, and those that follow, all the uncertain parameters excluded from \hat{p} are assumed to take on their nominal value. Table 1 presents the resulting PSMs. Recall that ρ_i measures the separation between the nominal operating conditions point and the failure domain corresponding to the i th requirement. The results are fairly intuitive. The worst-case requirement for Λ_{THL} , Λ_{RU} , Λ_{AL} , and δC_{nr} uncertainty is the yaw rate tracking requirement g_9 . Furthermore, δC_{lp} and δC_{ma} trigger unacceptable levels of high-frequency oscillation before compromising command tracking (i.e., the deviation leading to the violation of $g_7 < 0$ is smaller than the deviation for $g_2 < 0$, $g_3 < 0$, $g_4 < 0$ and $g_5 < 0$). The metrics in Table 1 will be used to compare the robustness of $U_{\text{nom}}(k_{\text{base}})$ with that of other controllers.

Multidimensional analyses led to the data in Table 2. The second and third columns show the aggregate PSM and a Monte Carlo estimate of the failure probability. The parameter η , which implies the combination of aerodynamic uncertainties $\delta C_{lp} = 0.8\eta$ and $\delta C_{ma} = \eta$, is used to evaluate the effects of the simultaneous pitch and roll uncertainties on the aircraft's performance. The factor 0.8 was subjectively chosen to make both δC_{lp} and δC_{ma} equally critical (see the geometry of the failure domain in Fig. 10). The metrics above enable the comparative analysis of competing control alternatives. With this aim in mind we postpone a discussion on the significance of these metrics to a later section.

Figure 10 shows the uncertain parameter space for $\hat{p} = [\delta C_{lp}, \delta C_{ma}]$. The coloring indicates the number of the requirements being violated. Therefore, whereas the safe domain is colored in white, the failure domain is colored in tones of gray. This figure, as some that follow, is generated by simulating the closed-loop response at the points of an uniformly spaced grid, calculating the constraint function g at each point, and counting the number of nonnegative components of each g . This exceedingly large number of simulations have only been made for illustrative purposes. The maximal set, whose calculation requires a few hundred evaluations of g , is superimposed. The separation between the maximal set and the failure domain indicates that the controller is more sensitive to δC_{lp} than to δC_{ma} . Furthermore, the almost rectangular shape of the safe domain indicates no interaction between these two uncertainties. This observation is in agreement with the control design procedure in which the longitudinal and lateral/directional controllers were designed independently. The CPV occurs when $\delta C_{ma} = 0$. Note that the physics at $\delta C_{ma} = 0$ and at $0 < \delta C_{ma} \ll 1$ differ significantly due to the 50% reduction in the elevators' effectiveness required to generate δC_{ma} . This figure, as those that follow, was calculated by performing simulations that start from the trim point. This is consistent with the manner in which the piloted simulations and flight experiments were run. In them, the controller was engaged after the vehicle was trimmed. The dependence of the closed-loop response on the initial conditions can be studied by making them part of the uncertain parameter vector \hat{p} .

Figure 11 shows the number of requirement violations for $\hat{p} = [\tau, \eta]$.** In contrast to Fig. 10, the geometry of the safe

**By definition, the CPV is a point on the surface of the maximal set that touches the boundary of the failure domain. Some of the figures misleadingly show that the CPV is at the interior of the safe domain. This is a mere consequence of the manner in which the figures are generated: they show a piecewise constant function over a uniform partition of the parameter space. The same value/color is assigned to all parameter realizations constituting an element of the partition. That value corresponds to the center of the box. The actual function, which is used when calculating the maximal deformation, may vary across any given parameter range.

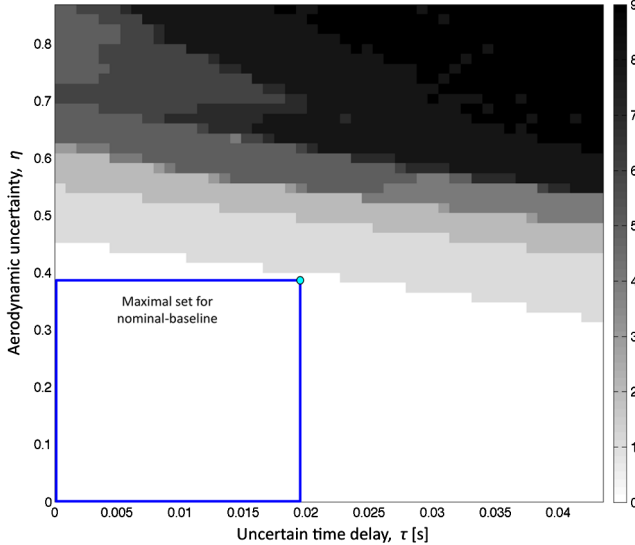


Fig. 11 Maximal set and failure and safe domains for $U_{\text{nom}}(k_{\text{base}})$.

Table 3 Relative PSM changes attained by $U_{\text{nom}}(k_{\text{tuned}})$ relative to $U_{\text{nom}}(k_{\text{base}})$

	$d\rho_1$	$d\rho_2$	$d\rho_3$	$d\rho_4$	$d\rho_5$	$d\rho_6$	$d\rho_7$	$d\rho_8$	$d\rho_9$
$\hat{p} = \Lambda_{\text{THL}}$	0	0	0	0	0	0	0	0	0
$\hat{p} = \Lambda_{\text{ELO}}$	0	0	0	0	0	0	0	-16	
$\hat{p} = \Lambda_{\text{AL}}$	0	0	0	-3	-2	-2	3	-3	-2
$\hat{p} = \Lambda_{\text{RU}}$	0	0	0	0	0	0	0	0	2
$\hat{p} = \tau$	0	0	0	0	0	0	0	0	0
$\hat{p} = \mu$	0	0	0	0	0	0	0	0	0
$\hat{p} = \Delta_x$	0	0	0	0	0	0	7	0	0
$\hat{p} = \delta C_{lp}$	0	45	0	48	35	45	59	0	34
$\hat{p} = \delta C_{ma}$	0	0	0	-8	0	0	0	0	0
$\hat{p} = \delta C_{nr}$	0	2	2	2	0	0	2	2	0

domain indicates that the system performance depends on the joint interaction of both uncertainties. This dependency, which appears to be linear, is driven by the reference tracking requirement on roll rate.

B. Nominal-Tuned Controller

The lateral/directional component of the nominal controller was tuned using the methods of Sec. IV.B. In particular, we searched for the Q and R matrices of the LQR-PI structure that maximize the PSM corresponding to $\hat{p} = [\delta C_{lp}, \delta C_{ma}]$ given the requirements above, as well as several stability and performance constraints at the nominal operating conditions point. This formulation enables incorporating robustness considerations to parametric uncertainties into the standard multi-input/multi-output LTI framework for control design. We have targeted the aerodynamic uncertainties δC_{lp} and δC_{ma} because the corresponding closed-loop response can be evaluated in both the high-fidelity simulation and the flight experiment. The resulting controller will be denoted as $U_{\text{nom}}(k_{\text{tuned}})$.

Table 3 presents the relative change in the PSMs attained by $U_{\text{nom}}(k_{\text{tuned}})$ relative to $U_{\text{nom}}(k_{\text{base}})$ for all requirements and all individual uncertainties. In this table, $d\rho_i$ is the PSM associated with $U_{\text{nom}}(k_{\text{tuned}})$ for the i th requirement in g minus that for $U_{\text{nom}}(k_{\text{base}})$. Positive values indicate a robustness improvement, and negative values indicate a loss. These metrics enable determining the relative advantages and drawbacks of using the tuned controller over the baseline according to particular requirements and uncertainties.

Even though $U_{\text{nom}}(k_{\text{tuned}})$ and $U_{\text{nom}}(k_{\text{base}})$ have the same longitudinal controller, their robustness to failure in the left-outer elevator differ. This is because the CPV for Λ_{ELO} is negative; therefore, it couples the longitudinal and lateral/directional dynamics. With the exception of the PSMs for δC_{lp} , which are largely improved, the PSMs for other uncertainties remain practically unchanged.

Figure 12 shows the nine requirement functions comprising g as a function of δC_{lp} for both the baseline controller and the tuned controller. The figure's caption relates each of the nine requirements with a line convention. Recall that the i th requirement is satisfied at the parameter realizations where g_i takes on negative values. At the nominal parameter point $\delta C_{lp} = 0$ all requirements are satisfied for both controllers. As the roll damping uncertainty increases the requirement functions vary. The worst-case requirement, which is the

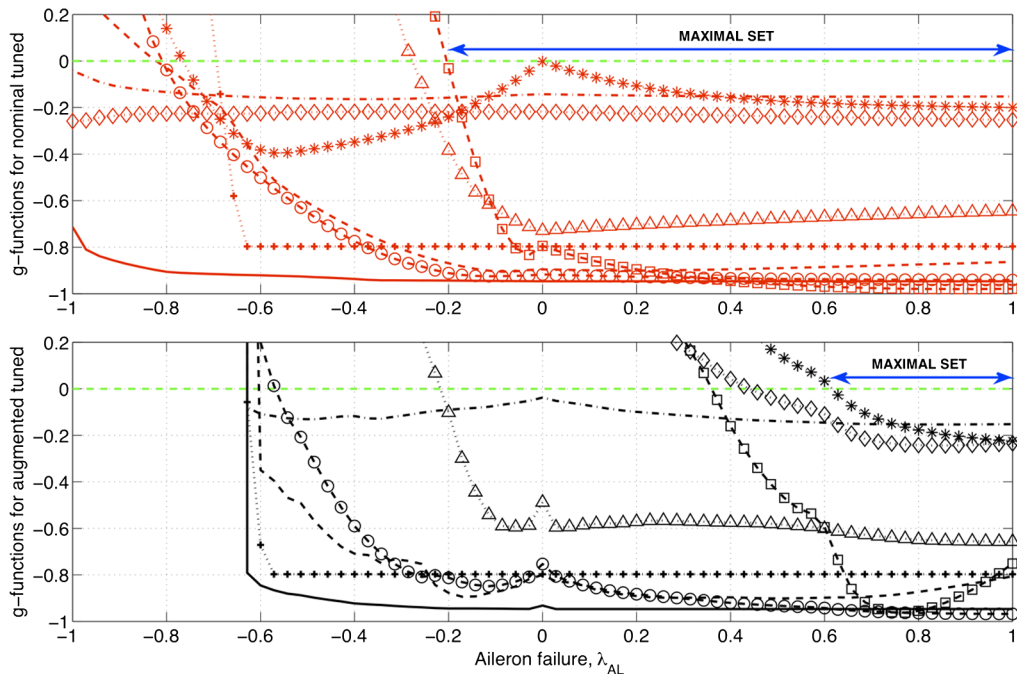


Fig. 12 Dependence of g on δC_{lp} for $U_{\text{nom}}(k_{\text{base}})$ and $U_{\text{nom}}(k_{\text{tuned}})$: g_1 (solid line), g_2 (square), g_3 (diamond), g_4 (asterisk), g_5 (triangle), g_6 (dash-dotted line), g_7 (dashed line), g_8 (circle), and g_9 (cross).

one that crosses $g_i = 0$ at the smallest value of δC_{lp} , is the one limiting the maximal set. The maximal sets are shown as left-right arrows. In this particular case the handling/ride quality requirement, g_7 , is the worst-case requirement for both controllers. Note that for the same requirement, the functions corresponding to k_{tuned} become positive at values of δC_{lp} that are much larger than those corresponding to k_{base} . This indicates that the robustness to uncertainty in δC_{lp} of the tuned controller is substantially better than that of the baseline.

Figure 13 shows the number of requirements violated by $U_{\text{nom}}(k_{\text{tuned}})$ as a function of δC_{lp} and δC_{ma} . The maximal sets corresponding to $U_{\text{nom}}(k_{\text{base}})$ and $U_{\text{nom}}(k_{\text{tuned}})$ are superimposed. Note that the tuned controller is able to tolerate 52% larger δC_{lp} uncertainties than the pilot-approved baseline controller. Robustness to δC_{ma} remains practically the same. Figure 14 shows the same information but applied to the joint aerodynamic uncertainty η and the time delay τ . The comparison of maximal sets and safe domains shows that the improvement in robustness to aerodynamic uncertainty does not degrade the time delay margin.

Table 4 shows the relative change in the PSM and the absolute change in the failure probability attained by $U_{\text{nom}}(k_{\text{tuned}})$ relative to $U_{\text{nom}}(k_{\text{base}})$ for the uncertainties in Table 2. Note that in most cases

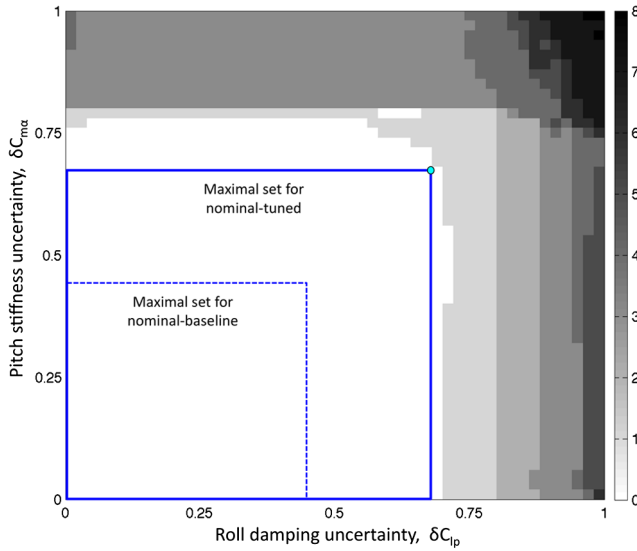


Fig. 13 Maximal set and failure and nonfailure domains of $U_{\text{nom}}(k_{\text{tuned}})$ for $\hat{p} = [\delta C_{lp}, \delta C_{ma}]$.

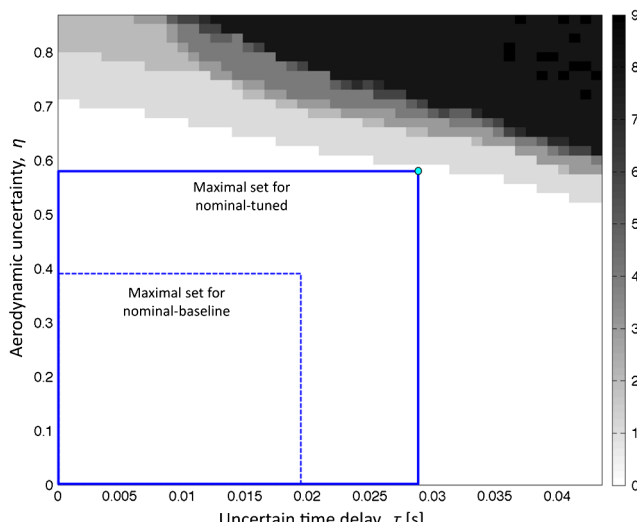


Fig. 14 Maximal set and failure and nonfailure domains of $U_{\text{nom}}(k_{\text{tuned}})$ for $\hat{p} = [\tau, \eta]$.

Table 4 Changes in PSMs and failure probabilities of $U_{\text{nom}}(k_{\text{tuned}})$ relative to $U_{\text{nom}}(k_{\text{base}})$

	$d\rho$	$dP[F]$
$\hat{p} = [\tau, \mu]$	-43	0.015
$\hat{p} = [\delta C_{lp}, \delta C_{ma}]$	51	0.344
$\hat{p} = [\Delta_x, \Delta_y]$	-9	-0.05
$\hat{p} = [\tau, \delta C_{lp}]$	49	0.230
$\hat{p} = [\tau, \delta C_{ma}]$	0	0.005
$\hat{p} = [\tau, \delta C_{nr}]$	0	0.03
$\hat{p} = [\delta C_{lp}, \delta C_{nr}]$	52	0.25
$\hat{p} = [\Lambda_{\text{THR}}, \Lambda_{\text{RU,RL}}]$	1	-0.02
$\hat{p} = [\tau, \eta]$	49	0.1
$\hat{p} = [\Lambda_{\text{ELO}}, \Lambda_{\text{ELI}}]$	0	-0.005
$\hat{p} = [\tau, \delta C_{lp}, \delta C_{ma}, \delta C_{nr}]$	33	0.265
$\hat{p} = [\Lambda_{\text{THR}}, \dots, \Lambda_{\text{RD}}]$	-24	-0.17

both metrics indicate similar trends. In other words, an increase (decrease) of the PSM commonly implies a proportional decrease (increase) in the failure probability. This is the case in all analyses with the exception of $\hat{p} = [\tau, \mu]$ where a reduction of 43% in the PSM does not yield a sizeable reduction in the failure probability. This situation arises because the failure domain has a long and thin spike intruding into the safe domain (not shown). This spike, whose existence will remain unnoticed to a Monte Carlo analysis with a moderate number of samples, bounds the maximal set. The spike is caused by a violation of the roll rate tracking requirement g_4 . Since the rate of change of g_4 within the spike is very low, the effects of this violation can be easily overcome by the pilot. Since the failure probability and the PSM are qualitatively different metrics of robustness, they may indicate different trends. Overall, the tuned controller exhibits a substantial improvement to δC_{lp} uncertainty at the expense of a moderate reduction in robustness to actuator failure.

The controller $U_{\text{nom}}(k_{\text{tuned}})$ was regarded suitable for flight after extensive evaluation by the pilot. Furthermore, piloted simulations at few realizations of δC_{lp} and δC_{ma} led to outcomes that were consistent with the observations made above. In addition, $U_{\text{nom}}(k_{\text{tuned}})$ was successfully validated using the NASA AirSTAR flight test vehicle. Details of the flight experiments, where nominal and offnominal flying conditions were evaluated, will be presented elsewhere. The augmented architecture proposed, having the nominal controller $U_{\text{nom}}(k_{\text{tuned}})$ at its core, will be tuned and analyzed in the following section.

VI. Augmented Controller

The parameters of the adaptive component are Q , θ_{\max} , Γ_1 , Γ_2 , and Γ_λ . Q prescribes the rate at which the Lyapunov function decreases in time, θ_{\max} prescribes the range of adaptation and Γ_1 , Γ_2 and Γ_λ determine the rate of adaptation.

The methods of Sec. IV.B were applied to determine Γ_1 and Q , which are the dominant controller's parameters. In particular, we searched for the matrices Γ_1 and Q that maximize the PSM corresponding to $\hat{p} = [\delta C_{lp}, \delta C_{ma}]$ such that $g(\bar{p}(\tau = 0.07)) < 0$; i.e., the nominal closed-loop system satisfies all the requirements when there is an additional time delay of 70 ms. This constraint helps balancing

Table 5 Changes in PSMs of $U_{\text{aug}}(k_{\text{tuned}})$ relative to $U_{\text{nom}}(k_{\text{tuned}})$

	$d\rho_1$	$d\rho_2$	$d\rho_3$	$d\rho_4$	$d\rho_5$	$d\rho_6$	$d\rho_7$	$d\rho_8$	$d\rho_9$
$\hat{p} = \Lambda_{\text{THL}}$	0	0	0	0	0	0	0	0	-2
$\hat{p} = \Lambda_{\text{ELO}}$	0	0	0	0	0	0	0	0	-19
$\hat{p} = \Lambda_{\text{AL}}$	-17	-17	-72	-78	-4	-3	-11	-14	-47
$\hat{p} = \Lambda_{\text{RU}}$	0	0	0	0	0	0	0	0	-2
$\hat{p} = \tau$	0	0	0	-13	0	0	-9	0	-15
$\hat{p} = \mu$	0	0	0	0	0	-7	0	0	-54
$\hat{p} = \Delta_x$	0	-7	0	-5	0	0	-6	0	-78
$\hat{p} = \delta C_{lp}$	0	-20	-30	-11	-13	-22	1	-19	-27
$\hat{p} = \delta C_{ma}$	0	0	0	-9	0	0	0	0	0
$\hat{p} = \delta C_{nr}$	0	-18	-22	-19	-12	-23	-18	-17	-21

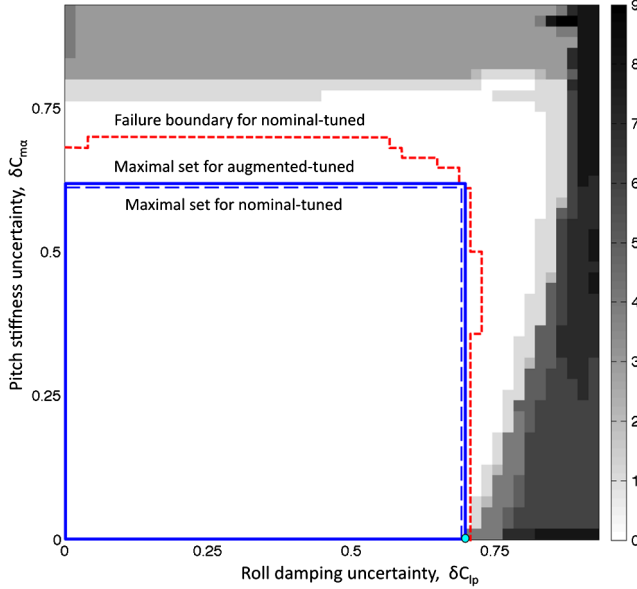


Fig. 15 Maximal set and failure and nonfailure domains of $U_{\text{aug}}(k_{\text{tuned}})$ for $\hat{p} = [\delta C_{lp}, \delta C_{ma}]$.

Table 6 Changes in PSMs and failure probabilities of $U_{\text{aug}}(k_{\text{tuned}})$ relative to $U_{\text{nom}}(k_{\text{tuned}})$

	$d\rho$	$dP[F]$
$\hat{p} = [\tau, \mu]$	57	$1e-1$
$\hat{p} = [\delta C_{lp}, \delta C_{ma}]$	1	$-8e-2$
$\hat{p} = [\Delta_x, \Delta_y]$	-51	$7e-2$
$\hat{p} = [\tau, \delta C_{lp}]$	-15	$1e-1$
$\hat{p} = [\tau, \delta C_{ma}]$	-2	$3e-3$
$\hat{p} = [\tau, \delta C_{nr}]$	-32	$1.7e-1$
$\hat{p} = [\delta C_{lp}, \delta C_{nr}]$	-22	$1.6e-1$
$\hat{p} = [\Lambda_{THR}, \Lambda_{RU,RL}]$	0	$-3e-3$
$\hat{p} = [\tau, \eta]$	7	$-9e-3$
$\hat{p} = [\Lambda_{ELO}, \Lambda_{ELI}]$	0	$3.5e-2$
$\hat{p} = [\tau, \delta C_{lp}, \delta C_{ma}, \delta C_{nr}]$	-8	$1e-1$
$\hat{p} = [\Lambda_{THR}, \dots, \Lambda_{RD}]$	-59	$2.4e-1$

the robustness to parametric uncertainties and time delays. Robustness analyses of the resulting controller, denoted hereafter as $U_{\text{aug}}(k_{\text{tuned}})$, are presented next. Table 5 presents $d\rho_i$, which is the PSM associated with $U_{\text{aug}}(k_{\text{tuned}})$ for the i th requirement in g minus that for $U_{\text{nom}}(k_{\text{tuned}})$, for a set of one-dimensional uncertainties. Note that reductions in the PSM occur in all but one of the cases. However, this case, which corresponds to the high-frequency oscillation requirement g_7 and the roll damping uncertainty δC_{lp} , is the worst-case requirement in the δC_{ma} - δC_{lp} space used for control tuning. Therefore, the 1% increase in the PSM of the worst-case requirement causes a sizeable reduction in the other ones.

Figure 15 shows the number of requirements violated by $U_{\text{aug}}(k_{\text{tuned}})$ as a function of δC_{lp} and δC_{ma} . Note that this is the space of uncertainties where the PSM is maximized. The maximal sets corresponding to $U_{\text{nom}}(k_{\text{tuned}})$ and $U_{\text{aug}}(k_{\text{tuned}})$, as well as the failure-domain boundary for $U_{\text{nom}}(k_{\text{tuned}})$, are superimposed. Even though the maximal set for $U_{\text{aug}}(k_{\text{tuned}})$ is slightly larger than that for $U_{\text{nom}}(k_{\text{tuned}})$, the safe domain associated with $U_{\text{aug}}(k_{\text{tuned}})$ is larger than the safe domain of $U_{\text{nom}}(k_{\text{tuned}})$. This improvement, which cannot be inferred from the one-dimensional PSMs in Table 5, indicates high sensitivity to the joint effect of the uncertainties.

Even though the robustness to δC_{lp} and δC_{ma} uncertainty was increased as intended, sizeable reductions in robustness to Λ_{AL} , τ , and δC_{nr} also occur (see Table 5).

Figure 16 shows the nine constraint functions constituting g as a function of $\hat{p} = \Lambda_{AL}$ for the nominal-tuned controller $U_{\text{nom}}(k_{\text{tuned}})$ and for the augmented-tuned controller $U_{\text{aug}}(k_{\text{tuned}})$. Recall that these functions assume negative values when the corresponding requirement is satisfied, and become positive when the requirement is violated. Note that at $\Lambda_{AL} = -0.62$, the value where the left aileron is stuck at 62% of its maximum deflection, all the requirement functions corresponding to $U_{\text{aug}}(k_{\text{tuned}})$ blow up. This phenomenon, which is solely caused by the adaptive component of the controller becoming unstable, occurs abruptly without any lead time for pilot reaction. This illustrates a serious drawback of adaptation in which the controller itself triggers instability. The elimination of this behavior requires smaller adaptive rates or smaller ranges of adaptation. Unfortunately, these actions mitigate both the advantages and disadvantages of adaptation. Table 6 shows the relative change in the PSMs and the absolute change in the failure probability attained by $U_{\text{aug}}(k_{\text{tuned}})$ relative to $U_{\text{nom}}(k_{\text{tuned}})$. These data indicate that the improvements in robustness to δC_{lp} and δC_{ma} yield a reduction in robustness to time delay, c.g. displacement, and actuator failure. The increase in the PSM corresponding to $\hat{p} = [\tau, \mu]$ results from the elimination of the spike mentioned above. The data in Table 6 are

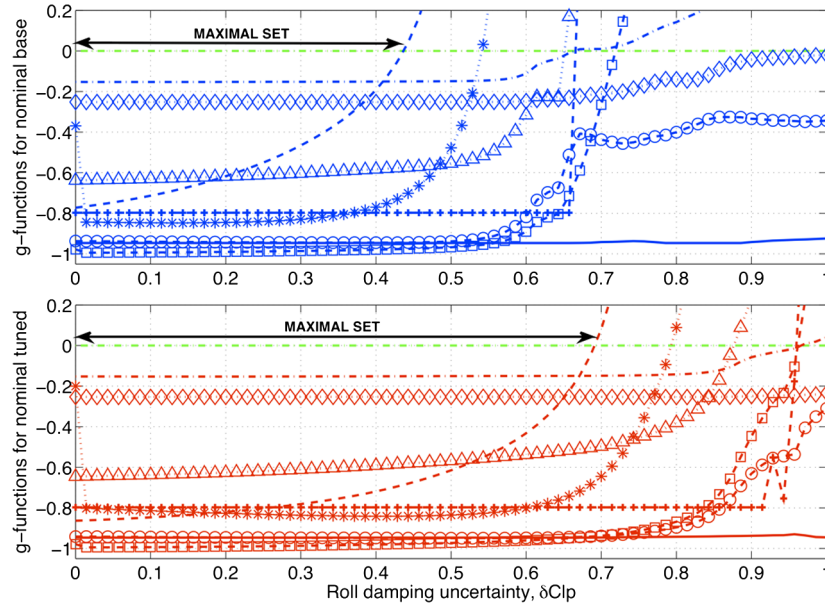


Fig. 16 Dependence of g on Λ_{AL} for $U_{\text{nom}}(k_{\text{tuned}})$ and $U_{\text{aug}}(k_{\text{tuned}})$.

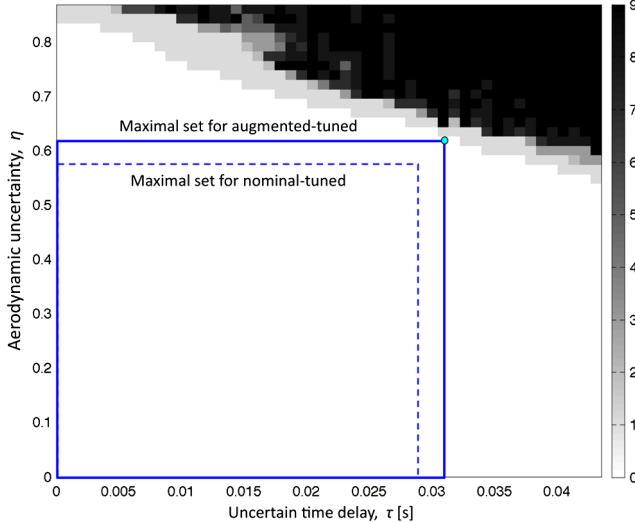


Fig. 17 Maximal set and failure and nonfailure domains of $U_{\text{aug}}(k_{\text{tuned}})$ for $\hat{p} = [\tau, \eta]$.

consistent with results from other optimization-based strategies where the optimal controller exhibits high sensitivity to those uncertainties that were left out of the problem formulation.

Figure 17 shows the number of requirement violations as a function of the uncertain time delay τ and the joint aerodynamic uncertainty η for $U_{\text{aug}}(k_{\text{tuned}})$. The corresponding maximal set, as well as that for $U_{\text{nom}}(k_{\text{tuned}})$ are superimposed (i.e., the maximal set in Fig. 14). Note that the safe domain and the maximal set corresponding to $U_{\text{aug}}(k_{\text{tuned}})$ are larger than those for $U_{\text{nom}}(k_{\text{tuned}})$. This indicates a beneficial effect of adaptation. Note, however, that

the region where all requirements are violated is dangerously close to the region where all requirements are satisfied. The closeness of these two regions suggests a transition to instability that may not be preceded by a noticeable degradation in closed-loop performance and that therefore may occur abruptly without any lead time for a pilot reaction. Further note that the separation between these two regions for $U_{\text{nom}}(k_{\text{tuned}})$, which can be seen in Fig. 14, is much larger.

A. Sensitivity to the Adaptive Rate

Figure 18 shows the number of constraint violations in $\hat{p} = [\delta C_{lp}, \delta C_{ma}]$ for four adaptive controllers. These controllers only differ in the value of their adaptive rate Γ_1 . Note that as the controller becomes more aggressive, spikes of the failure domain start intruding into the safe domain along the horizontal and vertical axes. These spikes cause a reduction in the PSM to the extent that the maximal set is empty for the most aggressive controller (i.e., the controller does not satisfy the requirements under nominal flying conditions). Note that according to the PSM, the transition between 4Γ and 8Γ yields a significant loss of robustness. The very same transition yields a robustness improvement according to the failure probability for a uniform density function. As before, note the small separation between the safe domain of the most aggressive controller and the region where all requirements are violated. The closeness of these two regions pose a grave safety risk, since the transition to instability may not precede by an observable degradation in closed-loop performance and as such, it will be very difficult to predict or avert. Recall that this mode of instability is caused by adaptation. These features illustrate the risk of over-tuning the adaptive control parameters based on the performance at few uncertainty realizations, and highlights the need for evaluating robustness from a global perspective.

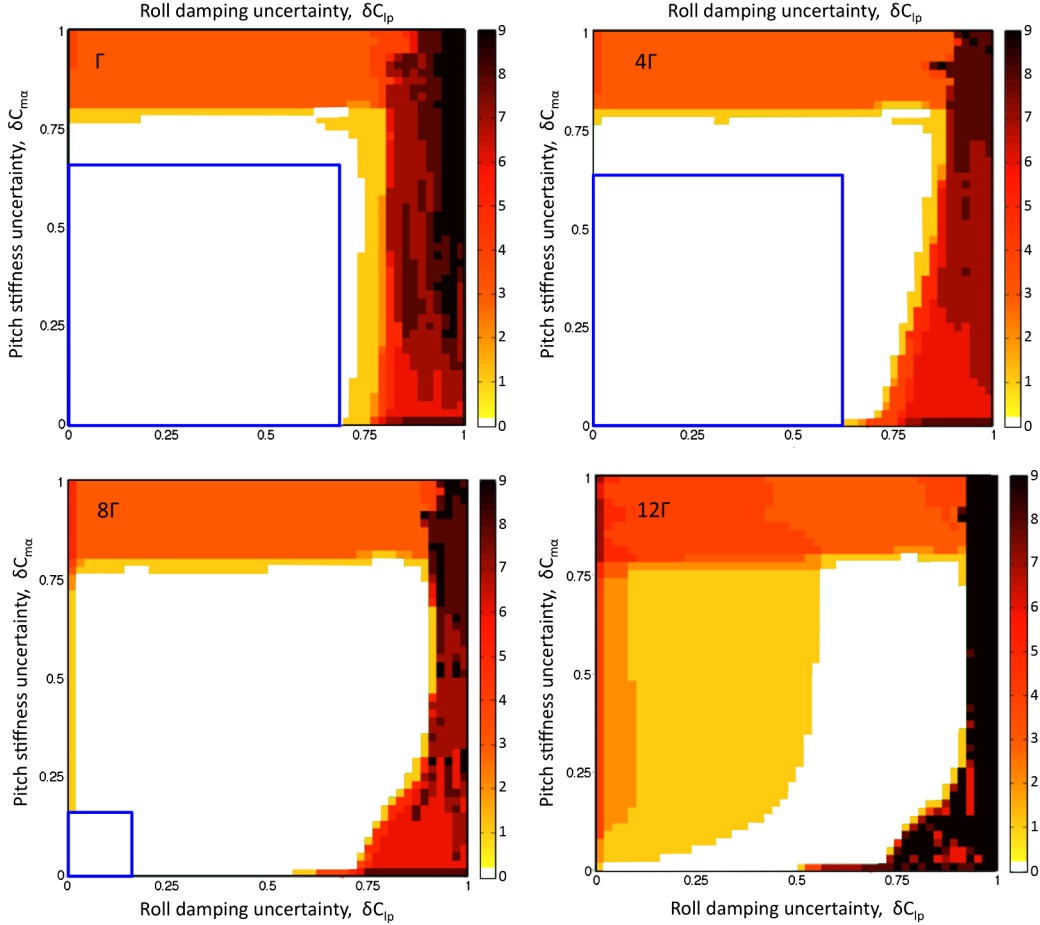


Fig. 18 Failure and nonfailure domains for increasingly larger adaptive rates.

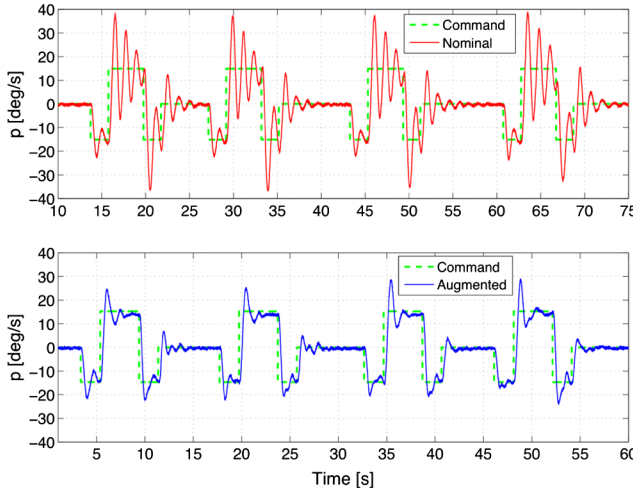


Fig. 19 Closed-loop responses corresponding to a train of roll rate commands.

B. Real-Time Simulation

Extensive piloted simulations were performed for several sets of flying conditions. In those conditions, not only the trim point at which the controller is engaged (e.g., wings-level flight at various airspeeds), but also the desired maneuver was varied. These maneuvers included coordinated turns, angle-of-attack captures, crab configurations, and offset landings. In the real-time simulation, and in contrast to the analyses above, the pilot commands \hat{r} are generated in real time according to the desired trajectory and the aircraft's response. Two licensed commercial, multi-engine, and instrument-rated pilots performed the piloted simulations and flight experiments. They have served as research pilots on several NASA remotely piloted vehicle research programs [8]. Furthermore, there is a more accurate aerodynamic model, a surface deadband in all control surfaces, sensor noise, and moderate turbulence.

Figure 19 shows the closed-loop responses corresponding to $U_{\text{nom}}(k_{\text{tuned}})$ and $U_{\text{aug}}(k_{\text{tuned}})$ when δC_{lp} and δC_{ma} make the open loop unstable. The improvement in the transient roll rate response attained by adaptation is apparent. Unfortunately, the unpredictability of the aircraft's response when flying at large bank angles disqualified $U_{\text{aug}}(k_{\text{tuned}})$ for a flight experiment in the NASA AirSTAR flight test vehicle. The root cause of this outcome is the unintended adaptation triggered by unmodeled dynamics in the reference model. Strategies to overcome this difficulty include expanding the range of accuracy of the plant in the reference model (e.g., use gain-scheduling, incorporate the nonlinear effects of gravity) and applying adaptive dead zones. These practices, for which some dynamics modeling is inexorably required, constitute a needed departure from the LTI framework supporting the theory.^{††}

VII. Conclusions

This paper presents the end-to-end procedure used to design an adaptive controller for a remotely operated air vehicle. The aim of this procedure, which encompasses both theoretical and practical considerations, is to develop an adaptive controller suitable for flight. A robustness analysis framework, which sizes the set of adverse flying conditions for which the closed-loop requirements are met, indicates some advantages and potential drawbacks of model reference adaptive control. Furthermore, a computational approach that integrates a design-optimization technique into this analysis framework is used to search for the controller's parameters that yield the best robustness characteristics allowed by the control structure. Practical aspects of developing a flight control system, such as the need for accurately modeling the aircraft dynamics, the performance degradation caused by actuator anomalies, and the consequences of

^{††}Videos of the piloted closed-loop response under offnominal flying conditions are available at <http://research.nianet.org/~lgcrespo/gtm.html>.

prescribing overly demanding reference models are illustrated. While faster adaptive rates can improve robustness to aerodynamic uncertainties, they commonly yield a reduction in time delay margin. More important, suitable adaptation rates for some uncertainty realizations (i.e., rates for which the augmented controller well outperforms the nominal controller and improves safety) may turn out to be excessively high for other uncertainties (i.e., situations where the adaptive controller, and thereby the augmented controller and the aircraft, becomes unstable). This setting defines a tradeoff from where the adaptive rates and the adaptive ranges should be prescribed. Failure to do this properly may lead to MRAC controllers that compromise safety by adapting either too rapidly (i.e., situations where unmodeled dynamics, nonlinearities, and time delays trigger instability) or too slowly (i.e., situations where parametric uncertainty in the aerodynamics and loss of control effectiveness trigger instability). MRAC controllers that balance these two conflicting objectives in an effective manner will be able to realize the improvements predicted by the theory.

Acknowledgment

This work was supported by the NASA Research Announcement NNX08AC62A of the Integrated Resilient Aircraft Control (IRAC) project of NASA.

References

- [1] Narendra, K. S., and Annaswamy, A. M., *Stable Adaptive Systems*, 1st ed., Prentice-Hall, Englewood Cliffs, NJ, 1989, Chaps. 1–7.
- [2] Astrom, K. J., and Wittenmark, B., *Adaptive Control*, 2nd ed., Addison-Wesley, Reading, MA, 1994, Chaps. 1–13.
- [3] Landau, Y. D., *Adaptive Control: The Model Reference Approach*, 1st ed., Marcel Dekker, New York, 1979, Chaps. 1–10.
- [4] Ioannou, P. A., and Sun, J., *Robust Adaptive Control*, 1st ed., Prentice-Hall, Upper Saddle River, NJ, 1996, Chaps. 1–9.
- [5] Sastry, S. S., and Bodson, M., *Adaptive Control: Stability, Convergence, and Robustness*, 1st ed., Prentice-Hall, Englewood Cliffs, NJ, 1989, Chaps. 1–8.
- [6] Jordan, T. L., Foster, J. V., Bailey, R. M., and Belcastro, C. M., “AirSTAR: A UAV Platform for Flight Dynamics and Control System Testing,” AIAA Guidance, Navigation, and Control Conference, AIAA Paper 2006-3307, Keystone, CO, Aug. 2006.
- [7] Murch, A. M., “A Flight Control System Architecture for the NASA AirSTAR Flight Test Facility,” AIAA Guidance, Navigation, and Control Conference, AIAA Paper 2008-6990, Honolulu, Aug. 2008.
- [8] Cunningham, K., and D. G., Murri, D. E. C., and Riddick, S. E., “A Piloted Evaluation of Damage Accommodating Flight Control Using a Remotely Piloted Vehicle,” AIAA Guidance, Navigation, and Control Conference, AIAA Paper 2011-6451, Portland, OR, Aug. 2011.
- [9] Crespo, L. G., Kenny, S. P., and Giesy, D. P., “A Computational Framework to Control Verification and Robustness Analysis,” NASA Langley Research Center, TP 2010-216189, Hampton, VA, 2010, pp. 1–38.
- [10] Dydek, Z. T., Jain, H., Jang, J., Annaswamy, A. M., and Lavretsky, E., “Theoretically Verifiable Stability Margins for an Adaptive Controller,” AIAA Conference on Guidance, Navigation, and Control, AIAA Paper 2006-6416, Keystone, CO, Aug. 2006.
- [11] Crespo, L. G., Matsutani, M., and Annaswamy, A. M., “Design and Verification of an Adaptive Controller for the Generic Transport Model,” AIAA Guidance, Navigation, and Control Conference and Exhibit, AIAA Paper 2009-5618, Chicago, 2009.
- [12] Matsutani, M., and Annaswamy, A. M., “An Adaptive Reset Control System for Flight Safety in the Presence of Actuator Anomalies,” *Proceedings of the American Control Conference*, Baltimore, MD, 2010.
- [13] Pomet, J.-B., and Praly, L., “Adaptive Nonlinear Regulator: Estimation from the Lyapunov Equation,” *IEEE Transactions on Automatic Control*, Vol. 37, No. 6, 1992, pp. 729–740.
doi:10.1109/9.256328
- [14] Crespo, L. G., Matsutani, M., and Annaswamy, A., “Verification and Tuning of an Adaptive Controller for an Unmanned Air Vehicle,” AIAA Guidance, Navigation, and Control Conference, AIAA Paper 2010-8403, Toronto, Aug. 2010.
- [15] Crespo, L. G., Munoz, C. A., Narkawicz, A., Kenny, S. P., and Giesy, D., “Uncertainty Analysis via Failure Domain Characterization: Polynomial Requirement Functions,” *ESREL 2011*, Troyes, France, Sept. 2011.

- [16] Crespo, L. G., Giesy, D. P., and Kenny, S. P., "A Verification-Driven Approach to Control Analysis and Tuning," AIAA Guidance, Navigation, and Control Conference, AIAA Paper 2008-6340, Honolulu, Aug. 2008.
- [17] Crespo, L. G., Matsutani, M., and Annaswamy, A., "Design of a Model Reference Adaptive Controller for an Unmanned Air Vehicle," AIAA Guidance, Navigation, and Control Conference, AIAA Paper 2010-8049, Toronto, Aug. 2010.
- [18] Anderson, B., "Failures of Adaptive Control Theory and Their Resolution," *Communications in Information and Systems*, Vol. 5, No. 1, 2005, pp. 1–20.